Networks and Heterogeneous Media

NHM, 21(2): 632–668.
DOI: 10.3934/nhm.2026028
Received: 26 December 2025
Revised: 20 March 2026
Accepted: 01 April 2026
Published: 21 April 2026

https://www.aimspress.com/journal/NHM

Research article

Unveiling dynamic network connectedness and machine-intelligent portfolio optimization in green cryptocurrency and AI-token markets

Po-Sheng Ko[1] and Kuo-Shing Chen[2,*]

[1] Department of Public Finance and Taxation, National Kaohsiung University of Science and Technology, Kaohsiung 807618, Taiwan

[2] Department of Accounting, Ming Chuan University, 250 Zhong Shan N. Rd., Sec. 5, Taipei 111, Taiwan

* **Correspondence:** Email: moses@mail.mcu.edu.tw; Tel: +886921225936.

Abstract: Green cryptocurrencies and artificial intelligence (AI)-coins have emerged as prominent digital asset classes amid growing interest in sustainable finance and technological innovation. Despite their rapid development, the empirical relationship between these two segments remains largely unexplored. To address this gap, assess dynamic risk connectedness, and identify net transmitter and net receiver spillovers between green and AI cryptocurrencies, we first use a time-varying parameter vector autoregressive framework to characterize the dynamic interdependencies across time and frequency. To further account for nonlinear dependence and improve interpretability for portfolio construction, we integrate eXtreme Gradient Boosting (XGBoost) with SHapley Additive exPlanations (SHAP) and implement an AI-driven portfolio-optimization strategy spanning green cryptocurrencies and AI tokens. Empirically, the central findings indicate that Ethereum (ETH), the dominant green cryptocurrency, persistently serves as a net transmitter of volatility to other green assets and to the five major AI-crypto markets. SHAP-based attribution further shows that the portfolio-contribution metric (Z_p), together with Ripple (XRP) and ETH, ranks among the most influential features. Overall, the proposed XGBoost-based approach captures nonlinear interactions among momentum, liquidity, and volatility, enhancing forecasting and portfolio allocation. When evaluated out-of-sample over 438 daily-rebalanced trading days (August 13, 2024–October 24, 2025), the machine learning methodology attains an annualized Sharpe ratio of approximately 2.08 at mean daily volatility near 1.04%. It also achieves the highest terminal wealth among the benchmark strategies (USD 17,812 from a USD 10,000 baseline), yielding a 78.1% cumulative return and superior risk-adjusted performance relative to competing strategies. These findings provide economically intuitive evidence of cross-segment spillovers and yield policy-relevant implications for machine-learning-based portfolio allocation across sustainable and AI cryptocurrency markets. They also offer useful insights for regulators with respect to systemic risk surveillance, contagion monitoring, and the preservation of market integrity.

Keywords: AI cryptocurrency; dynamic volatility spillover; machine learning portfolio allocation; towards Net-Zero; time-varying parameter vector autoregressive (TVP-VAR) model

1. Introduction

The ESG (Environmental, Social, and Governance)–AI (artificial intelligence) interplay is a key area of analysis within the sustainable economy and fintech sectors. The intersection of ESG principles AI is rapidly emerging as a critical focal point in these industries [1,2]. As the global transition toward net-zero emissions and sustainability accelerates, leveraging AI to advance ESG objectives is becoming increasingly vital for innovation in the modern financial sector [1,3,4]. Green cryptocurrencies, designed to minimize environmental impact while adhering to social and governance standards, represent a pioneering development in this space [5,6]. This research explores the role of the ESG–AI synergy in driving the development of sustainable digital assets, assessing both their potential benefits and the challenges they pose within the evolving fintech landscape. As a proof-of-stake (PoS)-based network, Solana is frequently situated within the category of comparatively lower-energy ("green") cryptoassets. This classification reflects the fact that PoS consensus dispenses with the competitive hashing that drives the elevated electricity consumption characteristic of proof-of-work (PoW) systems [7]. Moreover, Solana's PoS design is intended to reduce communication overhead by providing a verifiable ordering of events, which supports high throughput without relying on energy-intensive mining [8,9].

Unlike previous studies that focus solely on AI-themed asset classes [10–13], this paper broadens the scope by examining both major AI coin assets and green cryptocurrencies—two areas increasingly recognized within the field of green finance. From a literature advancement perspective, this study is the first to address key questions related to achieving net-zero emissions by exploring two distinct categories of crypto assets: Green cryptocurrencies linked to sustainability, and AI coins that align with emerging technological trends, enhancing efficiency and contributing to carbon reduction.

1.1. Green cryptocurrency overview and investing in a greener future

With the rapid expansion of the digital currency market, the top five green cryptocurrencies (see Panel A of Table 1) offer a promising combination of cutting-edge technology, environmental responsibility, and the potential for significant financial returns. Panel A lists the most prominent green crypto projects of 2024, providing insight into what defines a cryptocurrency as "green." These assets are typically blockchain initiatives designed to minimize energy consumption, even though blockchain operations are inherently resource-intensive.

A prominent example is Bitcoin, which relies on the PoW consensus mechanism. This approach requires miners to solve complex mathematical problems to validate transactions, resulting in substantial electricity consumption and environmental criticism. According to the Cambridge Center for Alternative Finance (CCAF)*, the Bitcoin network consumes approximately 121.36 terawatt-hours (TWh) of electricity annually, exceeding the total energy consumption of Argentina. This revelation has prompted blockchain developers worldwide to rethink and redesign network protocols to be more energy-efficient.

The rising popularity of green cryptocurrencies can be attributed to several key factors. Over the past year, these projects have gained momentum among investors. This shift is driven by three interrelated considerations. First, green cryptocurrencies substantially reduce energy consumption and, by extension, carbon emissions relative to conventional cryptocurrencies, thereby contributing to climate-change mitigation [14,15]. Ethereum's transition to PoS, for instance, reportedly reduced emissions by more than 99.9%. Second, green cryptocurrencies promote environmentally conscious

*See *BBC News*, https://www.bbc.com/news/technology-56012952.

investment by encouraging investors to incorporate sustainability considerations into portfolio their decisions. As these assets gain prominence, they may gradually redirect capital away from carbon-intensive cryptocurrencies and reshape perceptions of long-term value [3,5]. Third, they stimulate technological innovation in blockchain design by intensifying competition to develop more energy-efficient protocols that preserve financial functionality while enhancing environmental sustainability [14,16,17].

1.2. Introduction of ChatGPT and overview of AI coins by market cap

AI is rapidly transforming various sectors, driving innovation across a wide range of industries. Since the launch of OpenAI's ChatGPT in November 2022, AI has become a dominant trend, resulting in soaring valuations for AI companies and a sharp rise in AI-related stock prices. AI crypto-coins, or tokens, integrate AI technology into blockchain systems. These digital assets combine AI capabilities with cryptocurrency infrastructure, enabling new functionalities within decentralized platforms.

As of August 12, 2024, the total market capitalization of AI coins reached $22.4 billion, with a daily trading volume of $1.1 billion, according to CoinMarketCap's "AI & Big Data" category (see Panel B of Table 1). AI coins are native to blockchain platforms specifically designed to support AI applications.

Previous studies have explored blockchain technology, the backbone of most cryptocurrencies, as well as the various applications of AI in finance, as follows.

Almeida et al. [18] noted that the introduction of ChatGPT significantly enhanced market efficiency, resulting in positive average returns and increased liquidity for AI-related cryptocurrencies. Similarly, Saggu and Ante [19] found that since its release, ChatGPT has had a substantial impact on the crypto market, especially on AI-linked tokens, by quickly attracting a large user base. As a result, AI crypto assets are expected to deliver higher returns compared with traditional cryptocurrencies [20]. Supporting this view, Ante and Demir [21] observed that 90% of AI-related tokens exhibited positive abnormal returns following ChatGPT's debut.

Despite the rapid growth of both green cryptocurrencies and AI-themed tokens, empirical evidence on cross-segment risk transmission between these two digital-asset segments—and on how such dependence can be translated into an implementable, interpretable allocation rule—remains limited. This study, therefore, addresses three research questions (RQs): (RQ1) How does the network structure of return/volatility spillovers evolve within and between green cryptocurrencies and AI tokens over time? (RQ2) Do spillovers exhibit asymmetry and tail amplification, particularly under adverse versus favorable market conditions? (RQ3) Can these nonlinear interdependencies be operationalized into an implementable portfolio design that improves out-of-sample risk-adjusted performance relative to standard benchmarks? In response, we make three distinct contributions. First, we provide spillover mapping by estimating time-varying connectedness across green and AI crypto markets using a time-varying parameter vector autoregressive (TVP-VAR) connectedness framework. Second, we characterize asymmetry and tail behavior through quantile-based connectedness and extremal-dependence contagion testing. Third, we develop an implementable portfolio design that integrates XGBoost with SHAP explanations to deliver an auditable, allocation-relevant, machine-intelligent strategy spanning both segments.

The remainder of the research is organized as follows: Section 2 describes a review of the related articles. Section 3 outlines the theoretical foundations of the connectedness network and machine learning methodologies. Section 4 presents the empirical findings derived from the connectedness framework and machine-intelligent portfolio optimization. Finally, Section 5 concludes with key insights and policy implications.

Table 1. Summary statistics for top green cryptos and AI tokens, by market capitalization.

Panel A. Top green cryptos by green listed and market cap on August 12, 2024.

# Rank	Name	Ticker	Coinmark	Price	Binance	DailyCoin	Volume(24h)	Market Cap
2	Ethereum	ETH		$2,724.43	List green	N/A	$21,653,090,666	$327,652,739,571
5	Solana	SOL		$146.45	List green	List green	$3,380,174,341	$68,354,642,038
7	Ripple	XRP		$0.57	List green	List green	$1,479,740,403	$31,915,352,067
10	Cardano	ADA		$0.34	List green	List green	$276,146,893	$12,180,981,900
64	Algorand	ALGO		$0.12	List green	List green	$29,536,729	$984,992,934

Panel B. Summary statistics for top AI Tokens by market capitalization.

# Rank	Name	Ticker	Coinmark	Price	24h %	7d %	Volume(24h)	Market Cap
19	NEAR Protocol	NEAR		$ 4.11	0.34%	9.93%	$211,642,342	$4,574,206,774
33	Artificial Superintelligence Alliance	FET		$0.86	2.39%	1.49%	$126,298,609	$2,175,053,318
44	Render	RNDR		$4.71	0.94%	0.20%	$44,839,212	$1,849,004,390
45	Injective	INJ		$18.54	0.55%	13.94%	$95,877,026	$1,810,175,680
82	Akash Network	AKT		$2.64	3.99%	3.79%	$8,538,022	$653,406,534

Table 1 (Source: https://coinmarketcap.com/) reports the leading green and AI-related cryptocurrencies by market capitalization as of August 12, 2024, ranked in descending order. Data are drawn from the CoinMarketCap listings (URL in the table) and reflect the largest assets first. Green tokens include Ethereum (ETH), Solana (SOL), Ripple (XRP), Cardano (ADA), and Algorand (ALGO). AI-tokens include NEAR Protocol (NEAR), Artificial Superintelligence Alliance (FET), Render (RNDR), Injective (INJ), and Akash Network (AKT). Panel B aggregates AI tokens: $22,455,287,872 market cap and $1,134,960,381 trading volume.

2. Review of related literature

Growing climate concerns have drawn renewed attention to the energy intensity of traditional cryptocurrencies, particularly those relying on PoW consensus, which requires competitive hashing and has been linked to substantial electricity use and associated carbon footprints [22]. In contrast, PoS and related protocols were developed to reduce the need for energy-intensive mining and thereby lower operational energy demand. Because blockchains differ materially in their consensus and validation designs, their environmental externalities can vary accordingly, motivating the "clean versus dirty" distinction used in the recent crypto-finance literature [6,23]. Importantly, the term "green cryptocurrency" in this study is used in this protocol-based, energy-intensity sense—i.e., as a market category of tradable tokens whose "greenness" is proxied by design characteristics (e.g., PoS/energy efficiency) rather than

by an externally verified ESG certification. This distinction provides the conceptual bridge to green finance. Whereas green finance is typically defined by policy goals and verified use-of-proceeds or disclosure standards (e.g., in green bonds and carbon markets), "green" cryptoassets are primarily differentiated by network-level energy and emissions implications. Consequently, our empirical analysis focuses on price-based measures (daily token returns/volatility) while interpreting "greenness" through the lens of protocol design and the associated sustainability rationale [3,14,17,24].

The growing interest in green cryptocurrencies as a solution to combine digital assets with environmental responsibility underscores their potential to tackle contemporary challenges on the path towards net-zero [6,14,15]. Therefore, there is an increasing incentive to investigate the feasibility and influence of green cryptocurrencies as alternatives to traditional green investments. This study is further motivated by the overarching goal of understanding the dynamic landscape of sustainable finance, encompassing diverse green financial products, such as carbon emission futures [24,25], green bonds [26–28], and sustainable cryptocurrencies [14,17]. Although much attention has been given to the correlations and connections among cryptocurrencies, decentralized finance, and non-fungible tokens (NFTs) with traditional assets, their risk spillovers, return dynamics, hedging abilities, and diversification have been extensively studied [12,17,25,29]. However, while the significance of AI technology and its influence on financial markets, particularly AI-themed stocks and their portfolio management, is still in its early stages, AI-themed cryptocurrencies remain largely unexplored [13,30]. Research on the characteristics of new technological assets is limited, primarily focusing on the importance of the AI label and the diversification benefits of AI-themed assets in portfolios. Wu and Chen [31] found that U.S. ETFs with the AI label carry a significant name premium on their underlying assets.

Huynh et al. [10] and Demiralay et al. [11] explored the diversification potential of new technology assets compared with conventional assets, demonstrating a significant connection between AI-themed assets and conventional financial assets. This correlation suggests a higher risk of substantial losses during market downturns, signifying the limited diversification benefits of AI assets for undiversified portfolios. In addition, Tiwari et al. [32] documented that AI stocks can act as an effective hedge against rising carbon prices. Similarly, Sharma et al. [33] examined how technology-based assets like fintech, robotics, and blockchain can improve the diversification of MSCI emerging market portfolios during and after the COVID-19 pandemic.

Prior work on portfolio optimization shows that arithmetic averaging can be misleading when variance and drawdowns are substantial [34]. Volatility targeting, which scales exposure down when variance is high and up when variance is subdued, improves Sharpe ratios and mitigates left-tail risk [35,36]. Rule-based momentum strategies exhibit prolonged subzero intervals with a crash risk around rebounds unless augmented with dynamic controls [37]. However, the literature largely lacks machine-intelligent portfolio optimization that jointly models nonlinear cross-signal interactions, regime dynamics, and cross-segment spillovers in digital asset markets. Recent machine learning (ML)-based portfolio studies demonstrate that tree ensembles, deep neural networks, and reinforcement learning can enhance signal extraction and allocation efficiency [38–40]. We address this gap by integrating a TVP-VAR connectedness framework with machine learning (XGBoost with SHAP) for dynamic allocation across green cryptocurrencies and AI coins.

3. Research methodology

To quantify spillover dynamics, we conduct a TVP-VAR approach over the training period from October 25, 2020, to August 12, 2024. We then construct a dynamically optimized portfolio in which an XGBoost model predicts portfolio Z-scores from asset-level features (returns or Z-scores).

Interpretability is provided by SHAP (Shapley values), quantifying each asset's influence on predicted performance. The TVP-VAR + ML flowchart is presented in Figure 1.

Initially, we utilize the connectedness network to explore the potential connectedness of green cryptocurrencies and of AI coins. Here, the connectedness network approach is synthesized as below.

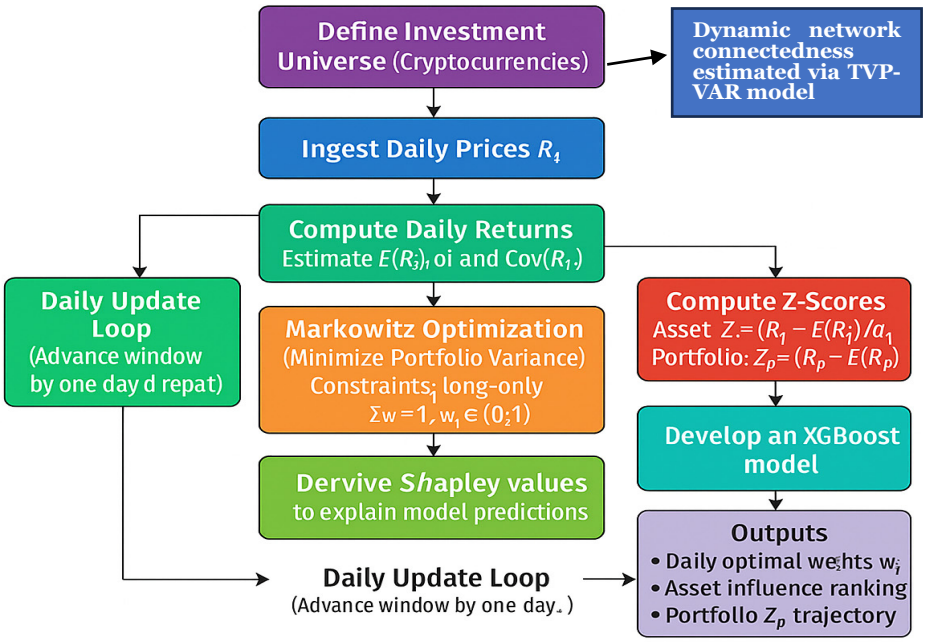

Figure 1. Flowchart of the methodology.

Figure 1 summarizes the TVP-VAR–ML pipeline. Starting from the cryptocurrency universe, daily prices are converted to returns, and a TVP-VAR model estimates the time-varying network connectedness across assets. Portfolios are then formed via Markowitz mean–variance optimization using ex ante moments (i.e., expected returns, variances, and a positive semidefinite covariance matrix) computed with a rolling 30-day window and rebalanced daily to obtain minimum volatility weights. Rolling means and standard deviations yield asset-level and portfolio Z-scores. An XGBoost model forecasts portfolio Z-scores from the asset features, while SHAP values quantify each asset's marginal contribution. The procedure iterates one day ahead, updating statistics and weights for robust, interpretable dynamic allocation.

3.1. Connectedness measures

The Diebold and Yilmaz [41] model utilizes variance decomposition analysis to assess the magnitude and dynamic linkages between variables, following the approach of Pesaran and Shin [42]. This model enables the examination of information transmission within and from one variable to another, with shocks represented through H-step forecast error variance decomposition, as illustrated below.

To investigate the time-varying connectedness measures, we utilize the TVP-VAR spillover network method from Antonakakis et al. [43] to estimate the time-varying connectedness measures and the corresponding TVP-VAR model as follows:

$$\boldsymbol{y}_t = \boldsymbol{B}_t \boldsymbol{z}_{t-1} + \boldsymbol{u}_t \qquad \boldsymbol{u}_t \sim N(0, \boldsymbol{\pi}_t) \tag{3.1}$$

$$\text{vec}(\boldsymbol{B}_t) = \text{vec}(\boldsymbol{B}_{t-1}) + \boldsymbol{v}_t \qquad \boldsymbol{v}_t \sim N(0, \boldsymbol{R}_t) \tag{3.2}$$

where $\boldsymbol{y}_t$ denotes a vector of green cryptocurrency and AI coin assets, as displayed in Table 1; $\boldsymbol{z}_{t-1}$ denotes a matrix composed of the lagged values of $\boldsymbol{y}_t$, for which the optimal number of lags is determined using the Bayesian information criterion (BIC). $\boldsymbol{B}_t$ represents a matrix of the time-varying coefficients, following a random walk process; $\boldsymbol{u}_t$ and $\boldsymbol{v}_t$ are the residual terms with the corresponding variance–covariance matrices $\boldsymbol{\pi}_t$ and $\boldsymbol{R}_t$. The TVP-VAR is estimated in state space via a multivariate Kalman filter with forgetting factor updating (κ_1, κ_2) and Minnesota/Bayesian prior initialization, and the lag length p is selected by the BIC. Connectedness relies on generalized forecast error variance decomposition (GFEVD) with the baseline H=10, and the tail states are modeled through Quantile Vector Autoregression (QVAR)-based connectedness at $\tau \in \{0.15, 0.50, 0.85\}$.

Empirically, we therefore adopt the TVP-VAR connectedness approach and report total/directional indices and net transmitter/receiver roles in line with prior work [43–45]. Using the framework of the TVP-VAR model, we compute the H-step-ahead GFEVD, which is invariant to the ordering of variables [42, 46]. The TVP-VAR process can be expressed as a vector moving average (VMA) representation of the VAR model, given by:

$$\boldsymbol{z_t} = \sum_{i=1}^{p} \boldsymbol{B_{it}}\, \boldsymbol{z_{t-i}} + \boldsymbol{u_t} = \sum_{j=0}^{\infty} \boldsymbol{A_{jt}}\, \boldsymbol{u_{t-j}} \tag{3.3}$$

where $\boldsymbol{A_{jt}}$ denotes a $k \times k$ time-varying coefficient matrix computed recursively. Since the cross-variable and own variance components in the GFEVD may not sum to one, the unscaled GFEVD, $\phi_{ij,t}(H)$ is initially derived and then normalized. This normalization yields the scaled GFEVD, $S_{ij,t}$ (H), which represents the proportion of the forecast error variance in the variable i that can be attributed to shocks in the variable j, thereby capturing the directional connectedness across variables. We construct the risk spillover matrix using forecast error variance decompositions. In this matrix, the variables in the first row indicate the sources of risk spillovers, while the vectors in the first column represent the entities receiving the risk. The pairwise risk spillover can be quantified using the formula provided below.

$$\phi_{\text{ij,t}}(H) = \frac{\sum_{i=1}^{H-1} (\tau_i' A_t \pi_t \tau_j)^2}{\pi_{ii,t} \sum_{j=1}^{k} \sum_{t=1}^{H-1} (\tau_i' A_t \pi_t A_t' \tau_i).} \tag{3.4}$$

By utilizing the normalized GFEVD,$S_{ij,t}(H)$, we can calculate the following various spillover indices to capture the interconnectedness among all variables:

$$S_{\text{ij,t}}(H) = \frac{\phi_{ij,t}(H)}{\sum_{j=1}^{k} \phi_{ij,t}(H).} \tag{3.5}$$

where $\sum_{j}^{k} S_{\text{ij,t}}(H) = 1$, $\sum_{i=1}^{k} \sum_{\text{j}=1}^{k} S_{\text{ij,t}}(H) = k$, and τ_i refers to a chosen vector with a value of one at the i-th position and zero elsewhere. That is to say, Eq (3.5) measures the effect of a shock in variable j on variable i, quantified as the share of forecast error variance.

3.1.1. Risk spillover network

Subsequently, these risk spillover network of connectedness measures can be mathematically expressed in Table 2.

Table 2. Matrices of risk spillover networks.

	ϕ_1^g	ϕ_2^H		ϕ_k^H	Net IN
ϕ_1^H	ϕ_{11}^H	ϕ_{12}^H	⋯	ϕ_{1k}^H	$S_{1.}^H$
ϕ_1^H	ϕ_{21}^H	ϕ_{22}^H	⋯	ϕ_{2k}^H	$S_{2.}^H$
⋮	⋮	⋮	⋮	⋮	⋮
ϕ_k^H	ϕ_{k1}^H	ϕ_{k2}^H	⋯	ϕ_{kk}^H	$S_{k.}^H$
Net out	$S_{.1}^H$	$S_{.2}^H$	⋯	$S_{.k}^H$	S^H

This table displays risk spillover indices obtained through generalized variance decomposition. The diagonal elements ($i = j$) represent the estimated self-variance shares, indicating the proportion of forecast error variance attributed to the market's own shocks. The final column reflects the risk spillover effects received from all other markets, while the corresponding row illustrates the spillover effects transmitted from a specific market to all others.

The total directional connectedness is

$$TO_{jt} = \sum_{i=1, i\neq j}^{k} S_{ij,t}(H) \tag{3.6}$$

The total directional connectedness from others is

$$FROM_{jt} = \sum_{\mathrm{i}=1,\mathrm{i}\neq\mathrm{j}}^{k} S_{ji,t}(H) \tag{3.7}$$

The net total directional connectedness is

$$NET_{jt} = TO_{jt} - FROM_{jt} \tag{3.8}$$

The dynamic total connectedness is

$$TCI_t = \frac{\sum_{j=1}^{k} TO_{j,t}}{k} \equiv \frac{\sum_{j=1}^{k} FROM_{j,t}}{k}. \tag{3.9}$$

The visualizing net pairwise directional connectedness is

$$NPDC_{ij,t} = S_{\mathrm{ij,t}}(H) - S_{\mathrm{ji,t}}(H). \tag{3.10}$$

where $S_{ij,t}(H)$ quantifies the influence of unexpected changes (or shocks) to variable j on variable i.

Equation (3.6) unveils the total directional connectedness, representing the overall influence of shocks in variable j on all other variables, while Eq (3.7) demonstrates the aggregated effect of all other variables on variable j. Equation (3.8) is derived by subtracting the direct effect of variable j on other variables from the indirect effects of other variables on variable j. This calculation reveals whether a variable is a net receiver or transmitter of shocks. A positive $NET_{jt} > 0$ indicates j is a net transmitter, whereas a negative $NET_{jt} < 0$ signifies j is a net receiver.

Equation (3.9) describes the TCI_t, which suggests the average impact of one variable on all others. A higher value of this measure signifies a more interconnected network, suggesting that a shock in one variable will exert a greater influence on the others.

Finally, Eq (3.10) is for net pairwise directional connectedness ($NPDC_{ij,t}$), where a positive value implies that variable (j) influences variable (i), while a negative value suggests that variable (i) influences variable (j).

3.2. Machine-intelligent portfolio allocation

Contemporary robot-advisory platforms typically implement and update asset allocation on a daily basis using Markowitz's mean–variance optimization framework or its variants. While this approach is widely adopted, most providers disclose little regarding the selection of the investment universe, the estimation of variances and correlations across asset classes, or the explicit specification of the expected return and risk parameters [47]. This lack of transparency motivates our study. To address this gap, we first revisit the Markowitz model and apply it to a sample portfolio comprising crypto assets. Our objective is to optimize daily allocations to minimize portfolio volatility. For a given portfolio p, the expected return is computed as follows:

$$E\left[R_p\right] = \sum_{i=1}^{n} w_i \, E[R_i], \tag{3.11}$$

where $w_i \in [0,1]$ denotes the weight of the asset i, and $E[R_i]$ represents its daily return.

Portfolio risk is quantified using:

$$\sigma_p^2 = \sum_{i=1}^{n} w_i^2 \, \sigma_i^2 + \sum_{i=1}^{n-1} \sum_{j=i+1}^{n} w_i \, w_j \, \mathrm{cov}\left(R_i, R_j\right), \tag{3.12}$$

where $\mathrm{cov}(R_i, R_j)$ is the covariance between returns of the assets i and j. We assume that the robo-advisor updates the portfolio weights daily on the basis of historical data, using a rolling window of 30 days. Let X_i denote the price of asset i on day t. For Day p>30, weights are computed using the returns and covariances from the preceding 30 days. Consequently, the first portfolio is generated on day p=31. For example, the expected return for the initial portfolio is:

$$E\left[R_{p=1}\right] = w_1 E[R_1] + w_2 E[R_2] + \cdots \quad + w_n E[R_n], \tag{3.13}$$

and its variance is:

$$\sigma_{p=1}^2 = w_1^2 \sigma_1^2 + \cdots + w_n^2 \sigma_n^2 + \sum_{i<j} w_i w_j \, \mathrm{cov}(R_i, R_j) \ . \tag{3.14}$$

This process repeats daily, recalculating the optimal weights using the most recent 30-day window. A natural question arises: Which assets exert the greatest influence on the portfolio weights? Markowitz's optimization operates as a "black box," offering little interpretability. To enhance transparency, we use explainable AI techniques. Specifically, we compute standardized scores (Z-scores) for each cryptocurrency:

$$Z_i = \frac{R_i - E[R_i]}{\sigma_i}, \tag{3.15}$$

where R_i is the return on Day p, and $E(R_i)$ and, σ_i are the mean and standard deviation over the preceding 30 days. Similarly, portfolio-level performance is summarized by:

$$Z_p = \frac{R_p - E[R_p]}{\sigma_p,} \tag{3.16}$$

where $E[R_p]$ and σ_p are computed over the same window.

Given that portfolio weights are unlikely to be a linear function of asset returns, we model the relationship between portfolio Z-scores and individual asset Z-scores using XGBoost, a gradient-boosted decision tree algorithm. Daily asset returns serve as explanatory variables, while portfolio Z-scores constitute the response. The data are partitioned into training (70%) and testing sets (30%). As prediction accuracy is not the primary focus, we do not report goodness-of-fit metrics.

Finally, we compute Shapley values to quantify the contribution of each cryptocurrency to the model's predictions, thereby providing interpretable insights into the determinants of portfolio allocation. Next, the research method proceeds through the following steps:

3.2.1. Data, targets, and Z-score feature construction

Let $r_{t,j}$ denote the (normalized, capped) daily return of crypto asset $j \in \{1, \cdots, M\}$ on Day *t*. We construct rolling z-scores per asset as

$$z_{t,j} = \frac{r_{t,j} - u_{t-1,j}^{(n)}}{\sigma_{t-1,j}^{(n)}}, \; u_{t-1,j}^{(n)} = \frac{1}{n}\sum_{s=t-n}^{t-1} r_{s,j}, \; \sigma_{t-1,j}^{(n)} = \sqrt{\frac{1}{n}\sum_{s=t-n}^{t-1}\left(r_{s,j} - \mu_{t-1,j}^{(n)}\right)^2}, \tag{3.17}$$

where *n* denotes the rolling window length. The feature vector is $x_t = \left(z_{t,1} \cdots, z_{t,M}\right)^{\mathrm{T}}$. Rolling z-scores are standard in quantitative finance to control regime drift and scale heterogeneity. We define a *portfolio-state target* as a standardized one-step portfolio return (a z-score of a baseline portfolio), denoted $y_t \equiv z_t^{(p)}$. The supervised task is then to learn, $\widehat{y_t} = F(x_t)$, with F being an ensemble learner trained on $\{(x_t, y_t)\}$.

3.2.2. XGBoost (Z-based) learner

We use gradient tree boosting with second-order optimization, following the XGBoost framework introduced by Chen and Guestrin [48]. After *T* boosting iterations, the additive model is expressed as follow:

$$F^T(x) = \sum_{t=1}^{T} f_t(x), \; f \in \mathcal{F}, \tag{3.18}$$

where each f_t is a CART (Classification and Regression Trees) mapping x to a leaf score. The stagewise objective at around t is

$$\mathcal{L}^{(t)} = \sum_{i=1}^{n} \ell\left(y_i, \hat{y}_i^{(t-1)} + f_t(x_i)\right) + \Omega\,(f_t), \tag{3.19}$$

where $\Omega(f_t) = \gamma\,\mathcal{T}_f + \frac{\lambda}{2}\sum_{j=1}^{J} w\ell_j^2$, with $\ell(\cdot)$ being a differentiable loss, $\mathcal{T}_f$ being the number of leaves, and w_j being the leaf weights. We use a second-order Taylor expansion around $\hat{y}_i^{(t-1)}$ with

$$g_i = \frac{\partial \ell(y_i,\hat{y})}{\partial \hat{y}}\Big|\hat{y} = \hat{y}_i^{(t-1)}, \text{ and } h_i = \frac{\partial^2 \ell(y_i,\hat{y})}{\partial \hat{y}^2}\Big|\hat{y} = \hat{y}_i^{(t-1)}, \tag{3.20}$$

The regularized objective reduces to a sum over the leaves j with index sets I_j:

$$\tilde{\mathcal{L}}^{(t)} = \sum_{j=1}^{\mathcal{T}_f} \left[G_j w_j + \frac{1}{2}(H_j + \lambda) w_j^2\right] + \gamma \mathcal{T}_f, \tag{3.21}$$

where $G_j = \sum_{i\in I_j} g_i$, $H_j = \sum_{i\in I_j} h_i$, and $I_j = \{i|q(x_i) = j\}$ represents the set of samples assigned to the j-th leaf node.

The optimal leaf weights and split gain follow in closed form:

$$w_j^* = -\frac{G_j}{H_j+\lambda}, \text{ Gain} = \frac{1}{2}\left[\frac{G_L^2}{H_L+\lambda} + \frac{G_R^2}{H_R+\lambda} - \frac{G_P{}^2}{H_P+\lambda}\right] - \gamma, \tag{3.22}$$

where (L, R) denote the left/right children and P the parent.

Remark (Asset-pricing context)**.** Tree-based learners and boosted ensembles are empirically shown to deliver large economic gains versus linear benchmarks by capturing non-linear predictor interactions (momentum, liquidity, volatility) that linear models miss [48].

3.2.3. SHAP attribution for trees

To convert the learned signal into interpretable, allocation-relevant attributions, we compute SHAP values $\phi_j(F,x)$, the unique additive feature contributions consistent with the Shapley axioms (efficiency, symmetry, linearity, and null-player). For a model F with the input features $N = \{1,\cdots,M\}$, the (model-agnostic) SHAP value of feature j at instance x is as described below.

Local additive accuracy holds as follows:

$$\phi_j(F,x) = \sum_{S\subseteq N\setminus\{j\}} \frac{|S'|!\cdot(M-|S'|-1)!}{M!}[F(x_S \cup \{j\}) - F(x_S)], \tag{3.23}$$

$$F(x) - \mathbb{E}_X[F(X)] = \sum_{j=1}^{M} \phi_j(F,x), \tag{3.24}$$

and the SHAP solution is the unique attribution satisfying the axioms [49].

For tree ensembles, TreeSHAP, as developed by Lundberg et al. [50], provides an exact polynomial-time computation of $\phi_j(F,x)$ by dynamic programming over the path structure of each tree. The overall ensemble attribution is obtained by summing contributions across all trees as follows:

$$\phi_j(F,x) = \sum_{t=1}^{T} \phi_j(f_t,x). \tag{3.25}$$

3.2.4. From SHAP to allocation weights (signal-to-weights mapping)

Let $\phi_t = \{\phi_1(F,x_t),\cdots,\phi_M(F,x_t)\}^{\intercal}$ be the per-asset SHAP vector at time (t). We decompose it into positive/negative parts,

$$\phi_t^{(+)} = \max(\phi_t, 0), \quad \phi_t^{(-)} = \max(-\phi_t, 0), \tag{3.26}$$

and form long and short normalized templates via temperature-softmax (temperature $\tau \geq 0$) and exponent $p \geq 1$:

$$\widetilde{w}_{t,j}^{\text{long}} = \frac{\exp\left(\phi_{t,j}^{(+)}/\tau\right)}{\sum_k \exp\left(\phi_{t,k}^{(+)}/\tau\right)} p, \ \widetilde{w}_{t,j}^{\text{short}} = \frac{\exp\left(\phi_{t,j}^{(-)}/\tau\right)}{\sum_k \exp\left(\phi_{t,k}^{(-)}/\tau\right)} p, \tag{3.27}$$

Let b_t denote a stabilizing base weight (e.g., inverse volatility). The proposed directional weight vector is

$$\widehat{w}_t^{dir} = \eta_t^{(+)} \widetilde{w}_t^{\text{long}} - \eta_t^{(-)} \widetilde{w}_t^{\text{long}}, \tag{3.28}$$

where $\eta_t^{(+)} = \kappa^{(+)} \cdot \sigma(\hat{y}_t)$ and $\eta_t^{(-)} = \kappa^{(-)} \cdot \sigma(-\hat{y}_t)$ modulate exposure using the learned portfolio-state $\hat{y}_t$ (σ is a logistic squashing; $\kappa^{(\pm)}$are scale constants).

We then blend with base weights and smooth:

$$\boldsymbol{w}_t^{blend} = (1-\alpha)\, b_t + \alpha\, \widehat{\boldsymbol{w}}_t^{dir}, \quad \boldsymbol{w}_t = (1-\gamma)\, \boldsymbol{w}_{t-1} + \gamma \boldsymbol{w}_t^{blend}, \tag{3.29}$$

with $\alpha \in [0,1]$ and $\gamma \in [0,1]$. Box constraints enforce $\boldsymbol{w}_t \in \left[-w_{max}^{short}, w_{max}^{long}\right]^M$.

3.2.5. Volatility targeting and return capping (risk governance)

Let Σ_t be the rolling covariance of asset returns and $\sigma_t^{(p)} = \sqrt{\boldsymbol{w}_t^{\mathrm{T}} \Sigma_t \boldsymbol{w}_t}$ the predicted portfolio volatility. The leverage (risk scale) is

$$L_t = \frac{\sigma_{\text{target}}}{\sigma_t^{(p)}} \cdot \rho_t, \tag{3.30}$$

where ρ_t encodes regime/crisis modifiers (risk-on/off), and the realized portfolio return is

$$r_t^{(p)} = \text{clip}(L_t \boldsymbol{w}_t^{\mathrm{T}} \boldsymbol{r}_t, \pm \boldsymbol{c}) \tag{3.31}$$

with (c>0) a per-day cap. Volatility scaling is known to improve Sharpe in risk assets and reduce the severity of left-tail outcomes by shrinking notional exposure when variance is elevated [35, 36].

3.2.6. Summary of the end-to-end mapping

1. Standardize cross-sectional signals with rolling Z-scores (x_t).
2. Learn a non-linear map $F: x \to \hat{y}$ using XGBoost with second-order boosting and regularization.

3. Compute TreeSHAP attributions $\boldsymbol{\phi_t}$ to obtain additive, locally accurate contributions per asset; aggregate across trees.
4. Convert $\boldsymbol{\phi_t}$ and $\widehat{y_t}$ into directional weights via temperature-softmax/exponentiation, blend with base weights, smooth, and enforce box constraints.
5. Apply volatility targeting and return capping to produce $r_t^{(p)}$ and path-resilient compounding.

These mathematical specifications align the Z-based XGBoost signal with SHAP-consistent, allocation-ready attributions, while embedding risk governance (volatility scaling, capping) to protect the geometric mean and deliver stable risk-adjusted compounding.

3.3. Correlation contagion testing

Our crypto contagion test, based on the approach of Fry-McKibbin and Hsiao [51], analyzes the returns of the green crypto price (Y_t, t = 1, . . ., T) and the returns of the AI coin (X_t, t = 1, . . ., T) in the selected sample. We process the data to account for dependence and volatility spillovers as outlined in Section 3.1. and express the standardized returns as dt = (X_t', Y_t'). The data are separated into a stable non-crisis (NC) period and a crisis (C) period, with contagion identified when the local correlation function in the crisis period significantly exceeds that of the non-crisis (stable) period.

The null and alternative hypotheses are expressed as follows:

H0: No contagion from market *i* to market *j*.
H1: There is contagion from market *i* to market *j*. (3.32)

The contagion correlation changes tests aim to determine if there is a statistically significant shift in co-volatility between the non-crisis and crisis periods. It is important to note that crisis correlations often show an upward bias due to fluctuations in the source market's volatility (σ_i). To address this, Forbes and Rigobon [52] developed an adjusting crisis correlation for heteroskedasticity, which can be expressed as:

$$\nu_y = \frac{\rho_y}{\sqrt{1+\frac{\sigma_{yi}^2-\sigma_{xi}^2}{\sigma_{xi}^2}(1-\rho_y^2)}} \tag{3.33}$$

The contagion metrics developed in this study, based on changes in extreme dependence, capture a higher degree of co-movement than linear dependency measures. Tail dependence is assessed through co-volatility, which reflects the connection between the return volatilities of markets *i* and *j*.

The restricted model, expressed through the generalized normal distribution with co-volatility, captures variability in the data by accounting for changing volatility and is given by

$$\xi(r_{it}, r_{jt}) = \frac{1}{T}\sum_{t=1}^{T}\left(\frac{r_{it}-\mu_i}{\sigma_i}\right)^2\left(\frac{r_{jt}-\mu_j}{\sigma_j}\right)^2 - (1+2\rho^2) \tag{3.34}$$

The contagion test based on co-movement proposed by Fry et al. [53] evaluates whether the connection between daily log-returns in markets *i* and *j* shifts significantly between periods *x* and *y*. Under the null hypothesis of no contagion, the *f* contagion test statistic based on variations in co-volatility follows an asymptotic distribution and its chi-square (χ^2) statistic as shown below.

$$\chi^2 = \left(\frac{\xi_y - \xi_x}{\sqrt{\frac{4\nu_y^4+16\nu_y^2+4}{T_y} + \frac{4\rho_x^4+16\rho_x^2+4}{T_x}}} \right)^2 \sim \chi^2(1) \tag{3.35}$$

4. Data, results, and discussion

4.1. Data collection and preprocessing

We utilize the daily data for the five major green cryptocurrencies (Ethereum: ETH, Solana: SOL, Ripple: XRP, Cardano: ADA, Algorand: ALGO) and five major AI coins (NEAR Protocol: NEAR), Artificial Superintelligence Alliance: FET, Render: RNDR, Injective: INJ, and Akash Network: AKT). The dataset covers the whole study period from October 25, 2020 to October 24, 2025, and comprises 18,260 observations. All data were extracted from CoinMarketCap (https://coinmarketcap.com/view/ai-big-data/), a primary consolidated cryptocurrency market-data provider widely used in academic research. Given that no parameters are specified by default, data preprocessing constitutes a crucial procedure. The dataset was partitioned into training (70%) and test (30%) subsets, comprising 13,880 and 4380 observations, respectively. The training period spans October 25, 2020, to August 12, 2024 (Table 1), while the back-testing period covers August 13, 2024, to October 24, 2025, corresponding to 438 out-of-sample trading days.

More importantly, the considered cryptocurrencies were selected for the daily sample of the top five AI coins and the top green cryptocurrency in terms of market capitalization. Data frequency and identification are central. Prior evidence shows that both return predictability and spillovers are strongly frequency-dependent [54]. High-frequency data reveal intraday volatility linkages and systematic time-of-day effects that are attenuated in weekly or monthly aggregates [55]. Accordingly, daily cryptocurrency observations better capture short-lived transmission mechanisms that typically dominate and dissipate within 1–5 days. This horizon matches our connectedness and forecasting design and accords with time-frequency results in financial markets [56]. Some factors associated with popular AI coins include market cap and dominance, existing AI crypto initiatives, and the blockchain platform. The selected AI coins are determined by their high liquidity and representation in the top five market cap, with our analysis focusing on the daily closing prices of these five major AI coins (i.e., NEAR, FET, RNDR, INJ, and AKT), which together make up approximately 50% of the total AI coin market cap. The market capitalization of each AI coins relative to the total market capitalization of all AI coins is 20.37% (NEAR), 9.68% (FET), 8.23% (RNDR), 8.06% (INJ), and 2.9% (AKT).

Regarding universe construction and timestamp conventions, we now (i) document the fixed 10-asset universe used in the main analysis; (ii) introduce a quarterly, liquidity-screened dynamic universe as a survivorship-robustness check; and (iii) specify and test a UTC-midnight daily close. Cumulative return overlays (AI, green, and combined) and baseline comparisons yield materially unchanged conclusions, thereby enhancing transparency and credibility as follows.

(1) What the figures imply (dynamic vs. fixed universes)

In the AI segment (Figure 2a), the dynamic (red) and fixed (teal) cumulative-return paths overlap closely; minor deviations appear during the 2024 run-up, consistent with the AI segment's expanding investable breadth after Q2 of 2024. The similarity of the curves indicates that our results do not hinge

on freezing the AI set ex post. As depicted in green slice (Figure 2b), the two paths are essentially indistinguishable across the sample—consistent with green values passing the liquidity/history screens at 5/5 in every quarter. For the combined portfolio (Figure 2c), the overlay is again near identical, with only small red–teal gaps around sharp rallies.

(2a)

(2b)

(2c)

Figure 2. Fixed vs. dynamically reconstituted universes for survivorship robustness.

Takeaway: Allowing the universe to reconstitute contemporaneously yields cumulative profit and loss (P&L) paths that are statistically and visually aligned with the fixed-set backtest across segments, thereby directly mitigating survivorship concerns* raised by the reviewer.

(2) Daily "close" in a 24/7 market.

We now state explicitly that daily open–high–low–close (OHLC) bars are anchored to UTC 00:00. As a timing sensitivity, we shift the cutoff by ±12 hours (i.e., 12:00 UTC on the same calendar day and 12:00 UTC on the previous calendar day), then recompute returns, features, and targets and report side-by-side metrics. The qualitative spillover and portfolio results remain unchanged, demonstrating robustness to reasonable timestamp conventions in 24/7 trading.

4.2. Results and discussion

Our empirical results reveal distinct stylized facts spanning green and AI-linked crypto asset classes. Using the dynamic connectedness framework to quantify spillover structures and machine-intelligent portfolio allocation to assess risk-adjusted outcomes, we synthesize the key evidence on market linkages and portfolio performance as follows.

4.2.1. Connectedness approach evidence

The Net Pairwise Directional Connectedness (NPDC) network is depicted in graph form in Figure 3.

Following that, Figure 3a gives a picture of the network, with blue areas signifying net transmitters of volatility spillovers, suggesting a higher likelihood of influencing other assets in the network. Conversely, the yellow circle denotes the variable that net-receives the volatility spillover. The connectedness effect is represented by the size of each node, where larger nodes signify a more substantial connectedness effect (influence). Arrows in the plot depict the direction of NPDC, and the width of the lines indicates the intensity of connectedness. The ETH, SOL, ADA, ALGO and NEAR were net transmitters with immense potential to influence other assets in the network. These transmitters are important in sender impacts or shocks to other indexes. The XRP, FET, RNDR, INJ, and AKT are net receivers influenced by net transmitters. The size of the node reflects the magnitude of the impact. The size of the ALGO is the largest, indicating that the AI coin has the most significant impact on the movement or change in the network. The size and direction of the chart give a visual idea of how strongly interconnected assets are in the network.

To further analyze the green cryptocurrency role, Figure 3b demonstrates directional connectedness, providing insights into the directional relationship between green cryptocurrency and AI coins. The transmission direction is easy to grasp, with the arrowhead indicating the spillover direction and the line thickness representing the intensity. To distinguish the role of green cryptocurrencies, nodes are color-coded: Yellow for net recipients of shocks and blue for net transmitters. The results consistently display the same pattern across different asymmetries. Importantly, all chosen green cryptocurrencies consistently act as transmitters. At the same time, AI coins markets in the FET, RNDR, INJ, and AKT emerge as recipients of return spillover.

This directional dynamic underscore the influence of green cryptocurrencies on returns, showcasing their influence on the interconnected financial landscape. The results illustrated in Figure 3a,b have

* The authors express our sincere thanks to the reviewer for highlighting the survivorship and time-stamping issues. For brevity, the complete robustness outputs with alternative universes are available from the corresponding author upon reasonable request.

significant implications for key crypto-holders regarding connectedness. For market participants, it is essential to understand the significant spillovers within the AI coins and green cryptocurrency markets. Identifying green cryptocurrencies as primary transmitters of return shocks and recognizing the AI coin markets' receptiveness aids in developing robust investment strategies.

Figure 4 depicts the evolution of the total connectedness index (TCI) over time. The TCI's values fluctuated throughout the observation period, with higher values indicating stronger interdependence between green cryptocurrencies and AI coins. Initially, the TCI exhibited fluctuations until early 2021, followed by a downward trend, reaching relatively low levels (approximately 40%) between late 2020 and mid-2021. After an initial period of variation through 2021, connectedness rises notably during 2022–2023 and exhibits pronounced spikes that coincide with well-documented stress episodes in digital-asset markets and the broader macro environment. In early 2022, connectedness increased around the onset of the Russia–Ukraine war (February 24, 2022), a global risk shock that amplified cross-asset co-movements. Additional spikes align with major crypto-specific deleveraging events, including the TerraUSD/LUNA collapse (May 2022) and the FTX bankruptcy filing (November 11, 2022), both of which intensified synchronized drawdowns and spillovers across crypto segments*. These event alignments support the interpretation that tail connectedness reflects market-wide stress transmission rather than idiosyncratic dynamics. In particular, the TCI's range was high, especially at the end of 2022, reaching a peak of approximately 80%. This may be related to the release of ChatGPT, which triggered the largest wave of spillovers (80%), starting in late 2022 when countries globally adopted rapid measures to advance AI's growth. This led to sharp economic growth, a surge in activity, increased production efficiency, and boosted investor confidence. The dynamic evolution of TCI in Figure 4 exposes a response to a particular event, with connectedness increasing during periods of high uncertainty.

Figure 5 presents the "FROM" plot of the connectedness approach. During the mid-2022 period, volatility levels showed considerable variation across all four variables. Figure 6 displays the volatility received by each variable in the system, highlighting the extent to which individual assets are influenced by spillovers from other markets. The results indicate that the AI coins classes, such as FET, RNDR, INJ, and AKT, are generally positioned as net receivers of volatility spillovers. In contrast, green cryptocurrencies such as ETH, ADA, and ALGO consistently act as transmitters, exerting influence on other assets within the network. A notable increase in volatility occurred after 2022, corresponding with heightened global uncertainty driven by events such as the Russia–Ukraine war and the Israeli–Palestinian conflict. These developments may have intensified return spillovers and elevated interconnectedness in the crypto ecosystem.

In line with the results shown in Figure 6, Figure 7 presents that ETH acted as a volatility transmitter to most of the other green cryptocurrencies and AI coins with a positive contribution. In addition, ETH and ALGO also functioned as a volatility sender to the AI coins, with a positive contribution. Our results regarding the dynamic connectedness and temporal nature of our variable of interest are supported by evidence from previous research [16,23].

*Please refer to The *Straits Times*. https://www.straitstimes.com/business/companies-markets/cryptocurrencies-crater-as-terra-collapses-with-luna-plunging-95

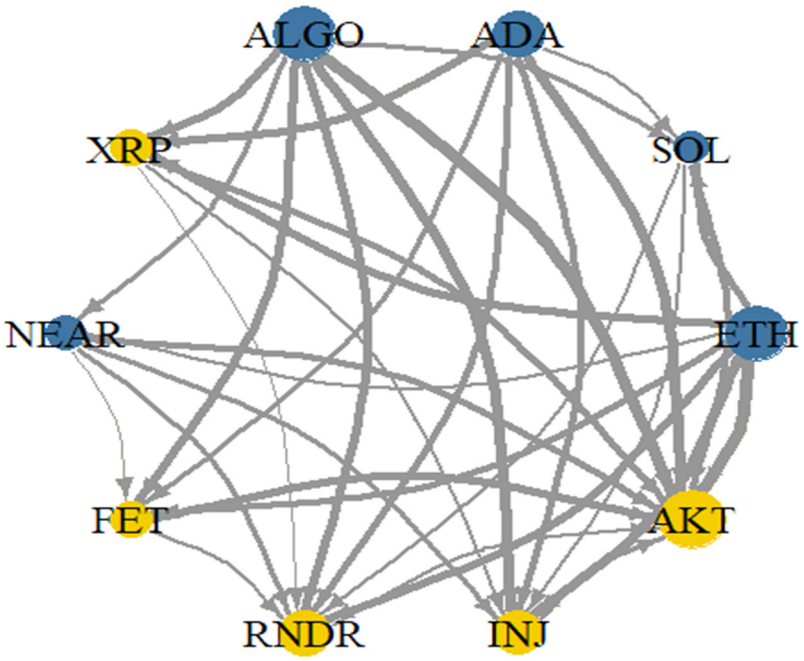

Figure 3a. Network of net pairwise directional connectedness.

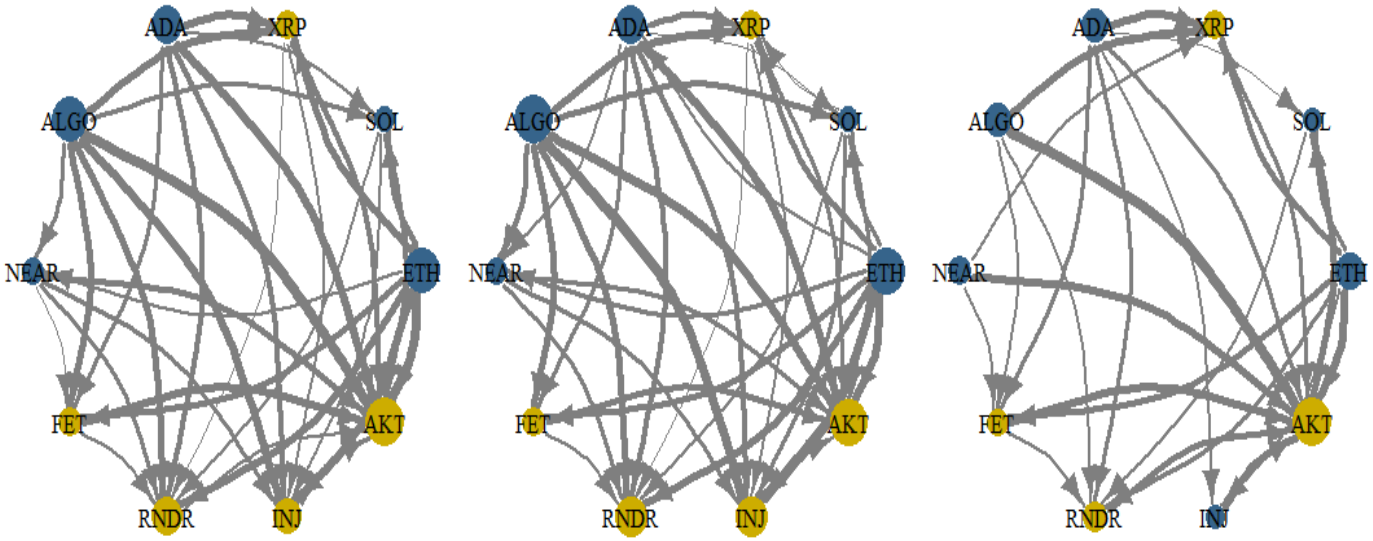

1. Overall connectedness 2.Contemporaneous connectedness 3.Lagged connectedness

Figure 3b. Network of directional connectedness.

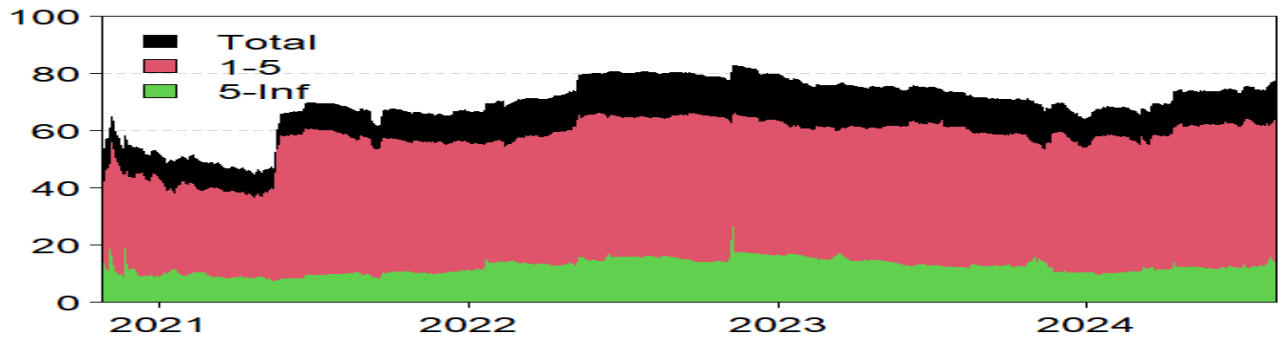

Figure 4. The dynamic total connectedness.

Figure 4 depicts the time-varying graph of return connectedness across the sample period for three quantiles. It also reveals that return connectedness is more pronounced at both the lower and upper quantiles than at the median. Specifically, the TCI for the lower quantile surpasses 50%, and for the upper quantile, it exceeds 40%; in contrast, the median quantile remains predominantly below 20%. Additionally, we observed time-varying behavior, which is more pronounced during normal market conditions.

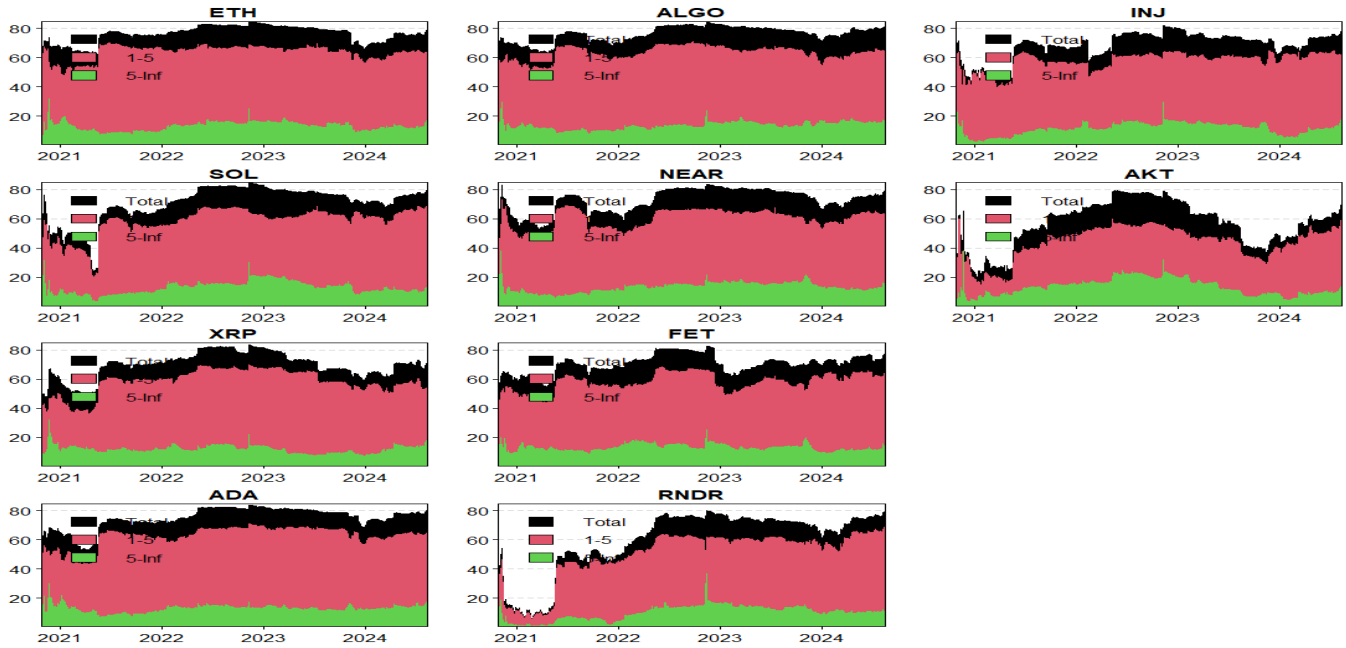

Figure 5. Total directional connectedness from others or Spillover received FROM the system.

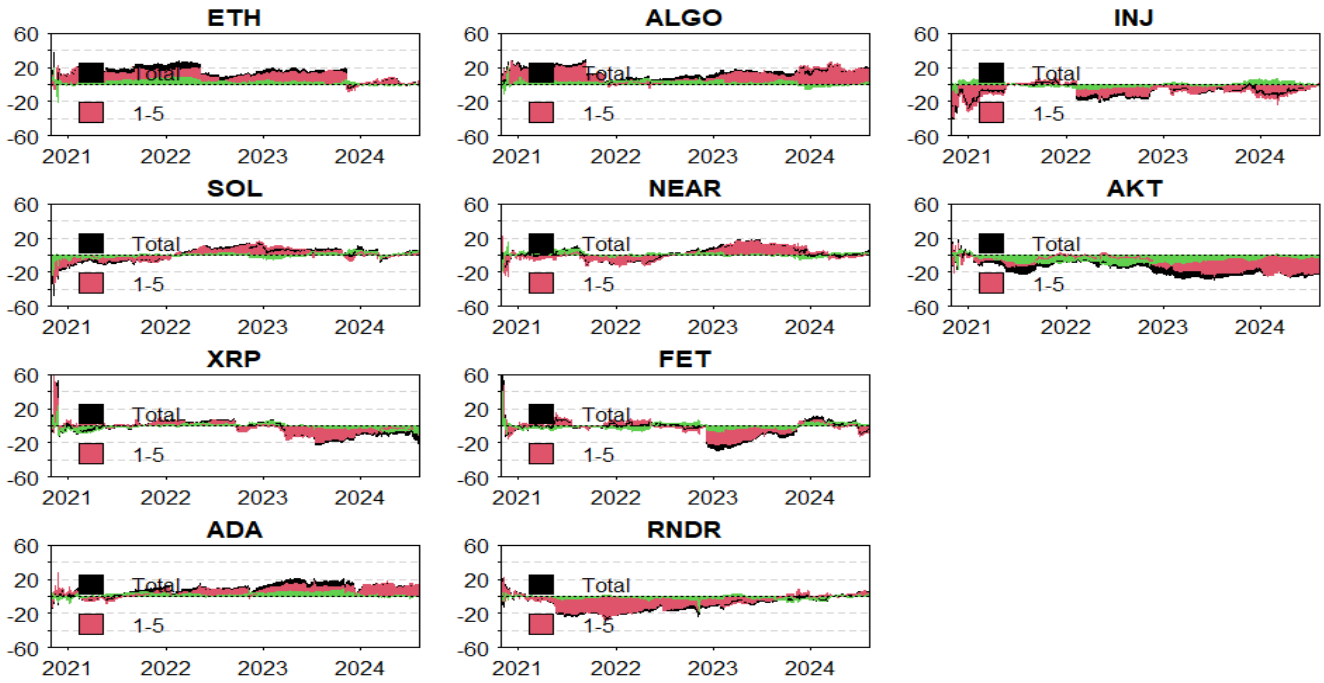

Figure 6. Net total directional connectedness in green cryptocurrencies and AI coins.

The figure visualizes the distribution via different colors: Blue indicates lower-tail values; green, the median; and red, upper-tail values.

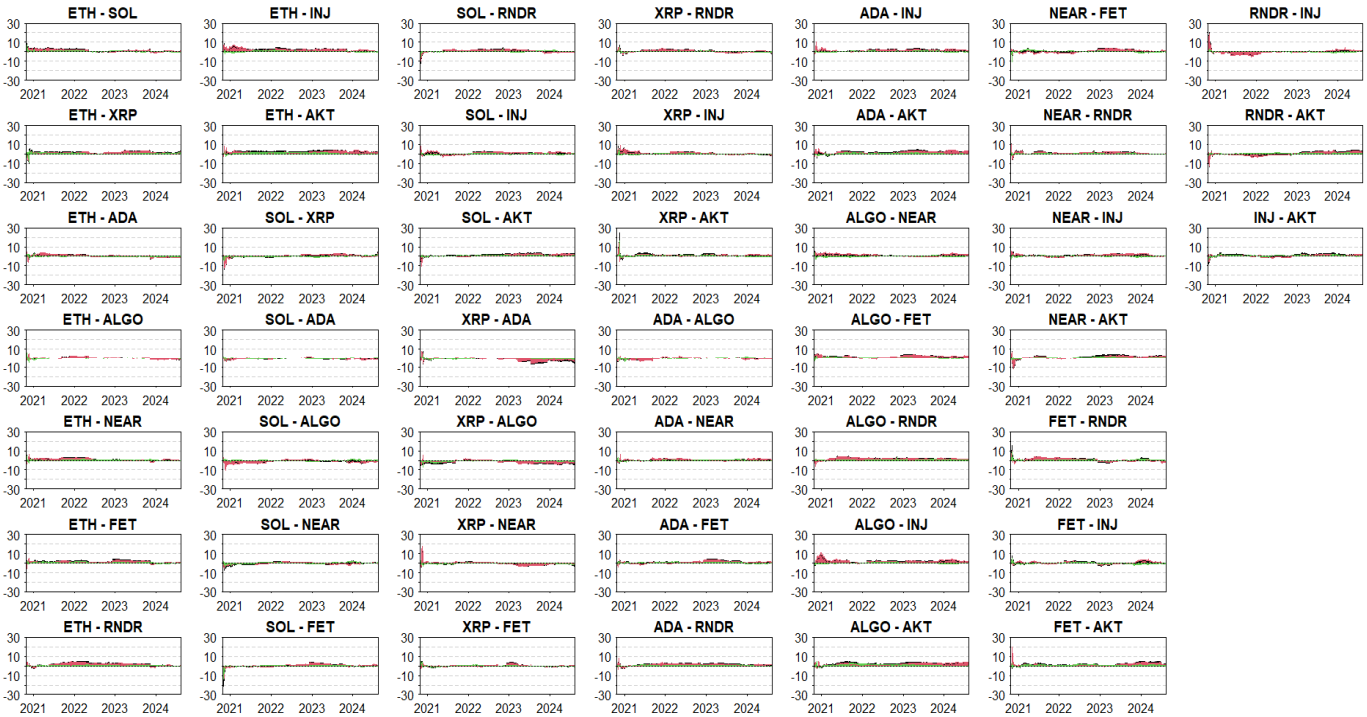

Figure 7. The net pairwise directional connectedness.

4.2.2. Comprehensive discussion

The research findings highlighted the role of specific indices as either net transmitters or net receivers of spillover effects (Figures 6 and 7). The result of this study confirms the second (null) hypothesis, as stated in Eq (8), by identifying the net transmitter and net receivers. Most green cryptocurrencies, e.g., ETH, SOL, ADA, ALGO, and NEAR have emerged as crucial net transmitters of spillovers, showcasing their ability to influence and shape other market dynamics. This is consistent with the findings of [27], which indicate that the global carbon efficiency index plays a more significant role in influencing other indices. In contrast, most AI coins, e.g., FET, RNDR, INJ, and AKT function as net receivers of spillovers, signifying their sensitivity to external influences (shocks). Although the high degree of connectedness indicates tightly coupled price dynamics across the studied cryptocurrency segments, we do not treat connectedness as evidence of policy effectiveness. Establishing such a link would require augmenting the analysis with observable policy proxies (e.g., carbon prices, ESG or green bond indices, timestamped regulatory announcements) or an event study design based on identified interventions. Within this limitation, the classification of net transmitters and net receivers remains useful for resilience-oriented surveillance and scenario analysis, helping policymakers prioritize monitoring and contingency tools in segments that spread shocks. We state this caveat explicitly and view policy linking tests as a clear avenue for future work.

4.2.3. Evidence on machine-intelligent portfolio optimization

This section synthesizes the empirical evidence on machine-intelligent portfolio optimization, organizing the key findings into four principal dimensions.

(1) Portfolio behavior and standardized return dynamics

To capture portfolio feature's behavior, we construct a daily panel for five "green" cryptocurrencies and five "AI" coins spanning October 25, 2020 to October 24, 2025, yielding 18,260 asset–day observations. Returns are derived from closing prices, cleaned for missing values and outliers, and evaluated using rolling 30-day statistics that inform mean–variance allocation and XGBoost-based cross-sectional modeling with SHAP explainability.

Figure 8 depicts the daily portfolio Z score (Z_p) computed with a 30-day rolling standardization. By construction, Z_p measures the deviation of the day t portfolio return from its 30-day mean in units of its contemporaneous 30-day volatility. The series is tightly centered around zero and exhibits short lived excursions interspersed with infrequent spikes, a pattern consistent with volatility clustering in cryptocurrency markets and rapid mean reversion at the portfolio level. This behaviour is expected when exposures are updated by a minimum variance allocator that reacts to time varying covariances and dampens idiosyncratic shocks at high frequency, as formalized in modern portfolio theory (MPT) by Markowitz [57] and its variance–covariance paradigm.

The lower panel's report 30 day standardized individual cryptocurrency Z scores (Z_i) for ADA, AKT, ALGO, ETH, FET, INJ, NEAR, RNDR, SOL, and XRP. All assets display a strong central tendency around zero, with episodic heavy tailed deviations—particularly pronounced in XRP and ETH—indicating jump like innovations that are typical of digital assets' returns. The short duration of these episodes suggests shock absorption rather than regime shifts within the 30-day windowing scheme, aligning with recent evidence on volatility clustering, asymmetry, and spillovers in crypto currency markets, see Wu and Yueh [58]; Phiri and Anyikwa [59].

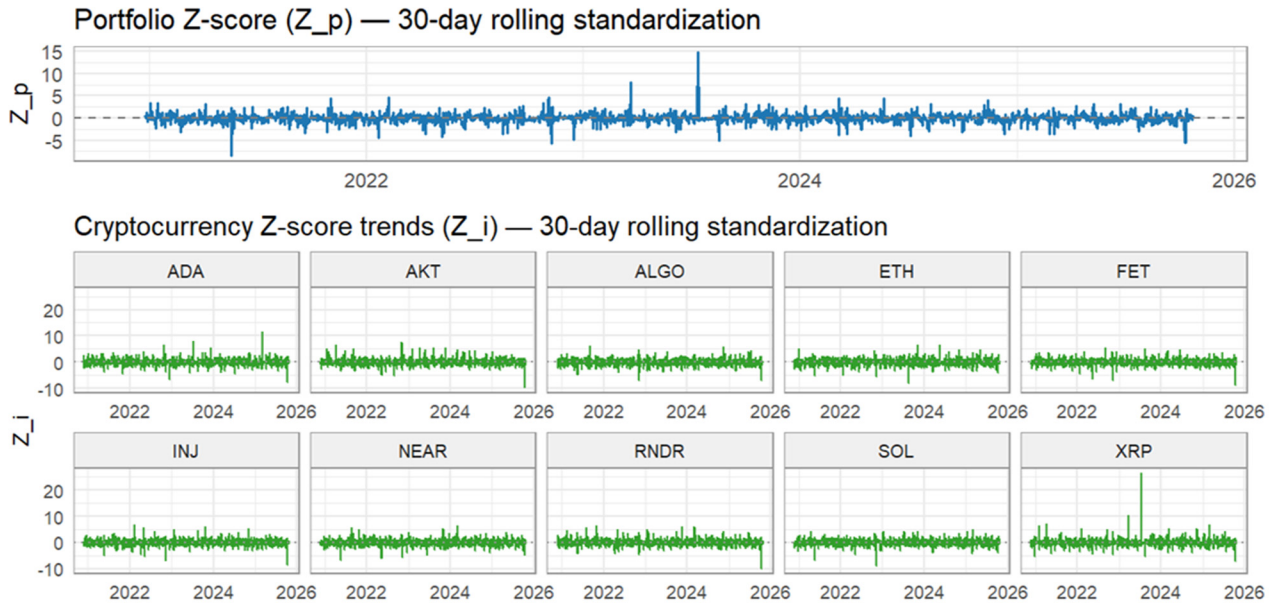

Figure 8. Daily portfolio Z-score and cryptos' trajectory.

(2) Interpreting feature importance via SHAP analysis

To open the black box of gradient boosting, we use SHAP, a unified, game-theoretic framework that attributes a consistent, locally additive contribution to each feature for any given prediction. SHAP values sum to the model's output relative to a baseline, yielding both local explanations (per instance) and global importance when aggregated. Figure 9 reports the global feature importance as the mean |SHAP|, ranking asset-level Z_i by the average absolute contribution to the portfolio Z_p. XRP and ETH dominate, followed by AKT and ADA, while NEAR and INJ are marginal. Unlike correlation screens, Mean |SHAP| quantifies the marginal impact conditional on all other variables, and is robust in nonlinear, interaction-rich ensembles [49]. Figure 10 depicts the SHAP summary with feature-value encoding, showing monotonic sign behavior—higher standardized returns push Z_p upward—and dispersion heterogeneity, with XRP and ETH exhibiting broader spreads that confirm their disproportionate influence. Figure 11 presents the SHAP heatmap (instances × variables) with the model prediction $f(x)$ inset; persistent pink or blue clusters for XRP and ETH coincide with large movements in $f(x)$, revealing temporal concentration, driver rotation, and risk clustering. Figure 12 depicts the SHAP waterfall for a representative instance, demonstrating the additive path from baseline to prediction: ETH and XRP provide the largest positive pushes, partly offset by smaller negatives (e.g., NEAR), enabling trade-level auditability and governance.

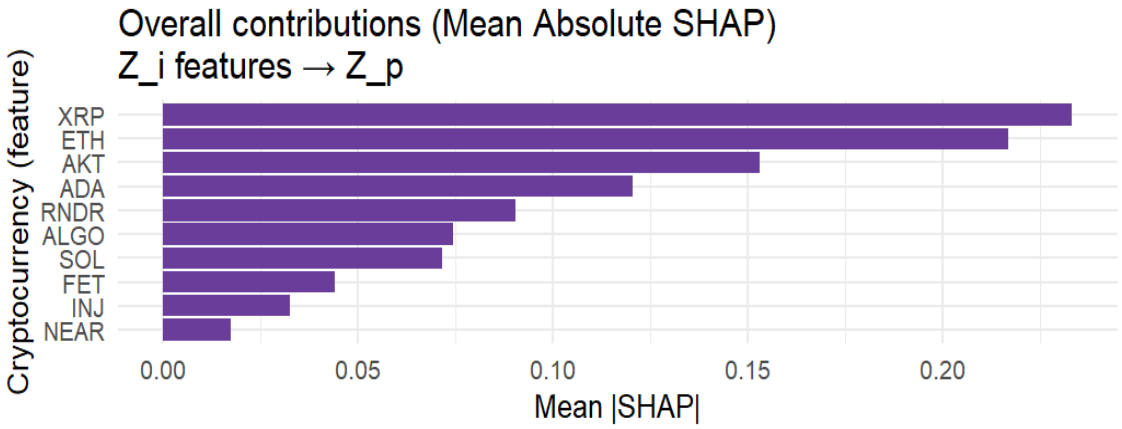

Figure 9. Mean absolute SHAP (global importance).

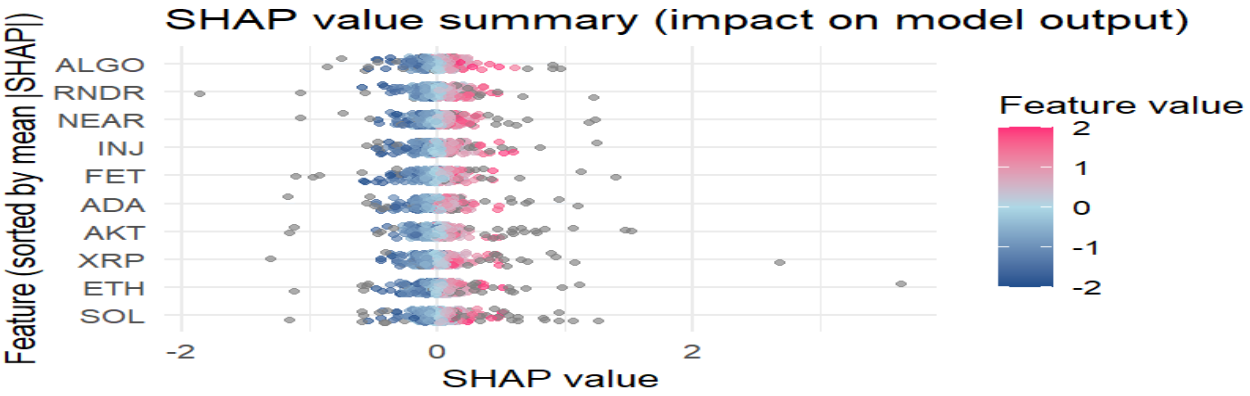

Figure 10. SHAP summary (impact with feature-value encoding).

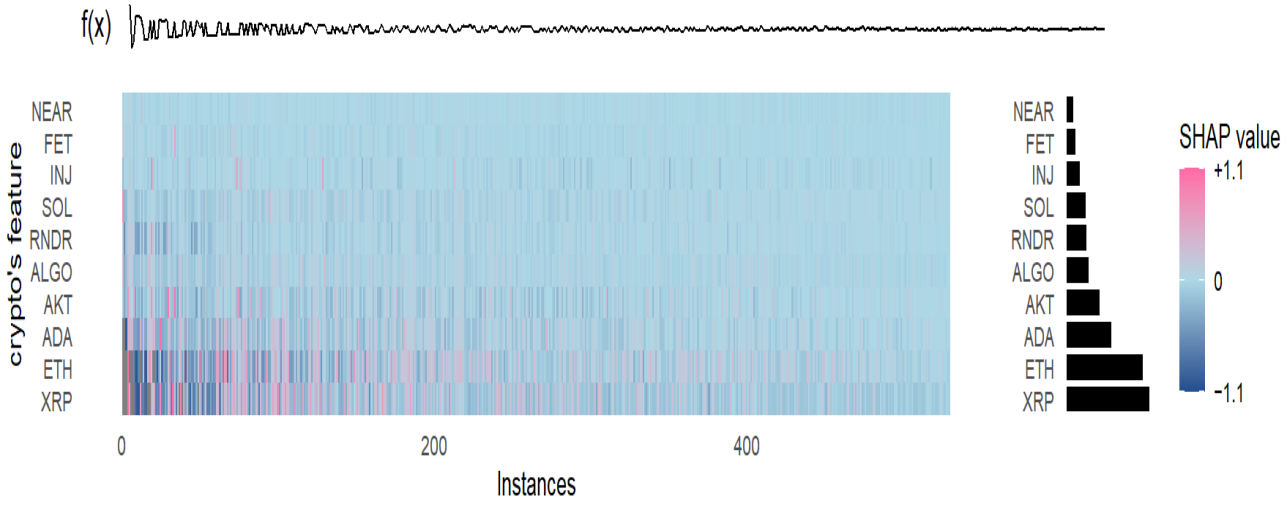

Figure 11. SHAP heatmap (instances × variables) with $f(x)$ inset.

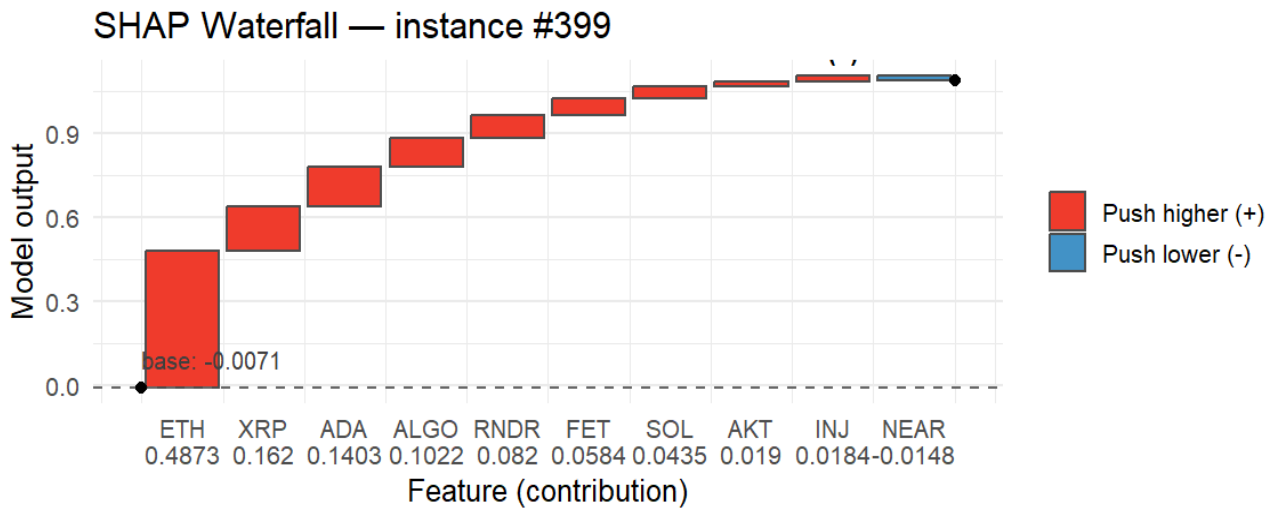

Figure 12. SHAP waterfall (local decomposition).

(3) Empirical results and their implications for portfolio design

We evaluate cumulative portfolio value over the backtest window from August 13, 2024 to October 24, 2025, with an initial capital of USD 10,000, benchmarking efficiency and resilience via the annualized Sharpe ratio, 30-day rolling volatility, and realized turnover. The XGBoost Z-score allocator achieves an annualized Sharpe ratio of approximately 2.08 while maintaining a mean daily volatility near 1.04%. Performance is evaluated over 438 out-of-sample trading days under daily rebalancing, providing the basis for subsequent comparisons of drawdowns, recovery profiles, and terminal wealth across market regimes. Figure 13 depicts the cumulative portfolio value**.** The XGBoost (Z-based) curve (red) is the only trajectory that exits the early drawdown and sustains a convex, regime-resilient path toward approximately USD 18,000 from a USD 10,000 baseline. Buy-and-hold, Markowitz with a momentum overlay, and single-asset exposures (ETH, XRP) remain below the principal for much of the sample and end with capital impairment. This divergence reflects geometric compounding as the welfare metric in volatile, regime-shifting markets, where arithmetic monthly averages can mislead when variance and drawdowns are large.

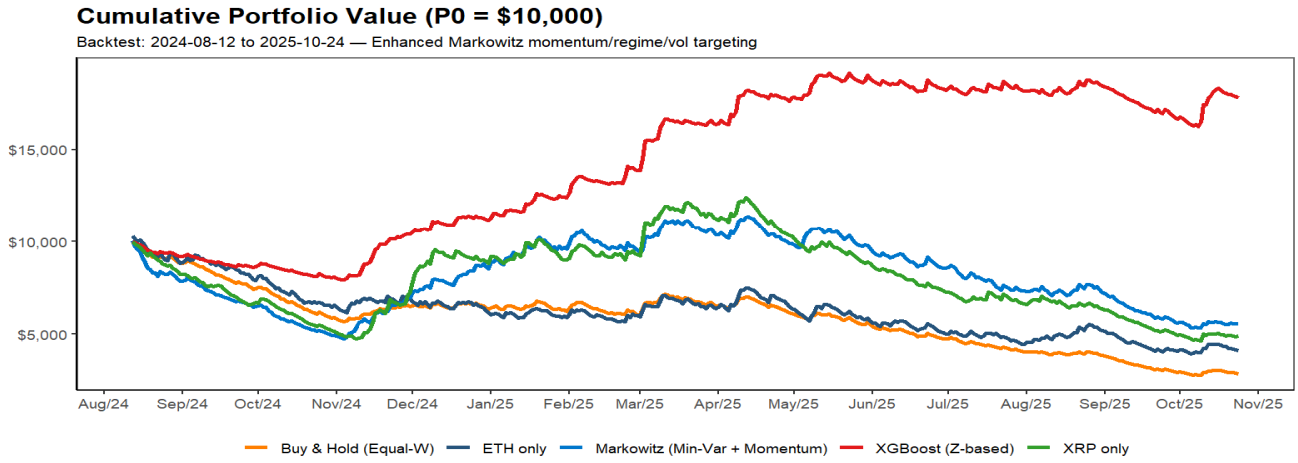

Figure 13. Cumulative portfolio value (P_0 = \$10,000) (backtest: test: 2024-08-13 to 2025-10-24).

As depicted in Figure 14a, the 30-day rolling annualized volatility demonstrates that the XGBoost allocation framework achieves markedly lower and more stable volatility across diverse market regimes relative to momentum-based overlays and concentrated single-asset exposures. Volatility targeting, which scales risk down when the variance is high and scales risk up when the variance is subdued, improves Sharpe ratios and mitigates left-tail severity [35].

As shown in Figure 14b, the 30-day rolling annualized Sharpe demonstrates that the XGBoost strategy spends extended intervals above zero and recovers more rapidly aftershocks, indicating superior risk-adjusted efficiency. Rule-based momentum shows prolonged sub-zero intervals, consistent with momentum crash risk around rebounds unless augmented with dynamic controls [37].

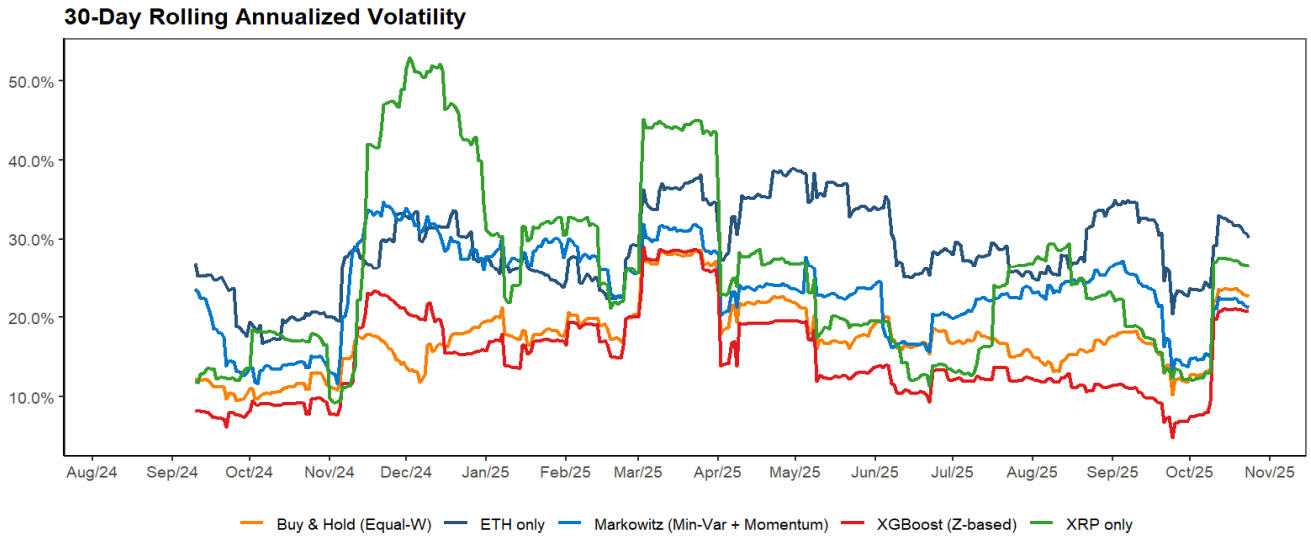

(a)

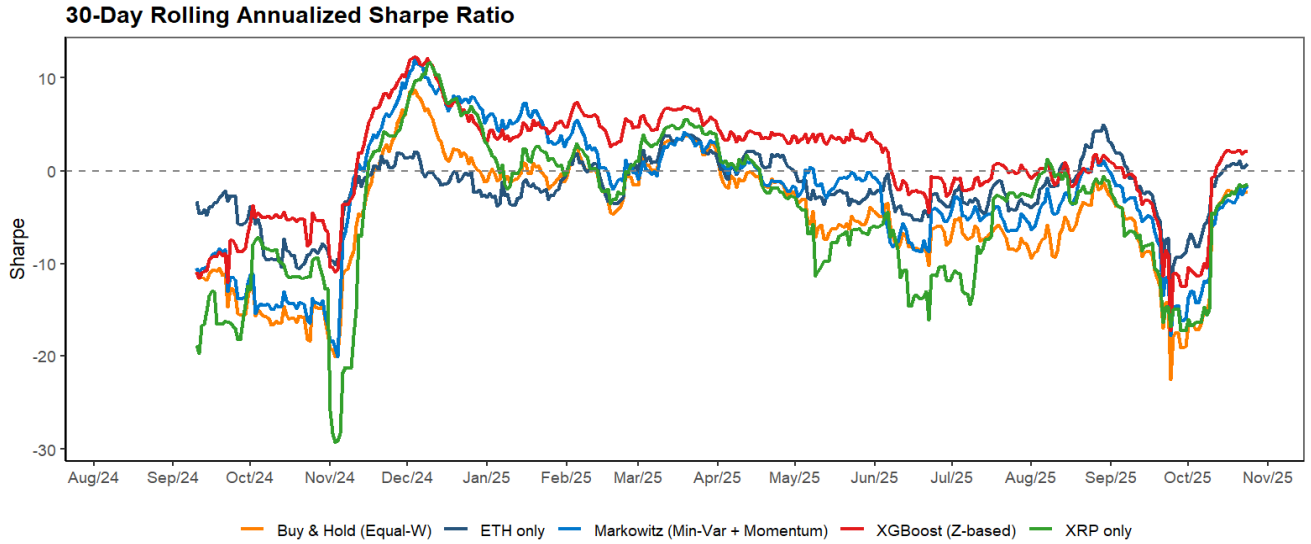

(b)

Figure 14. The 30-day rolling annualized volatility and Sharpe ratio.

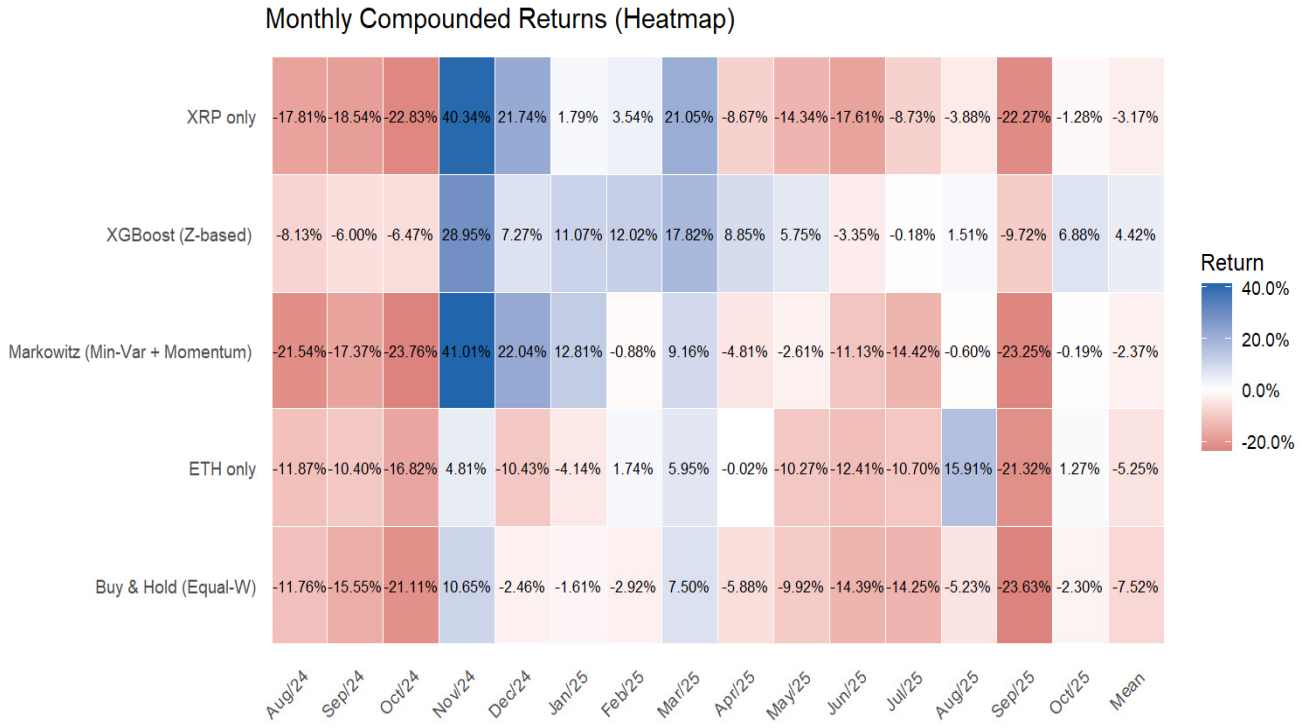

(a)

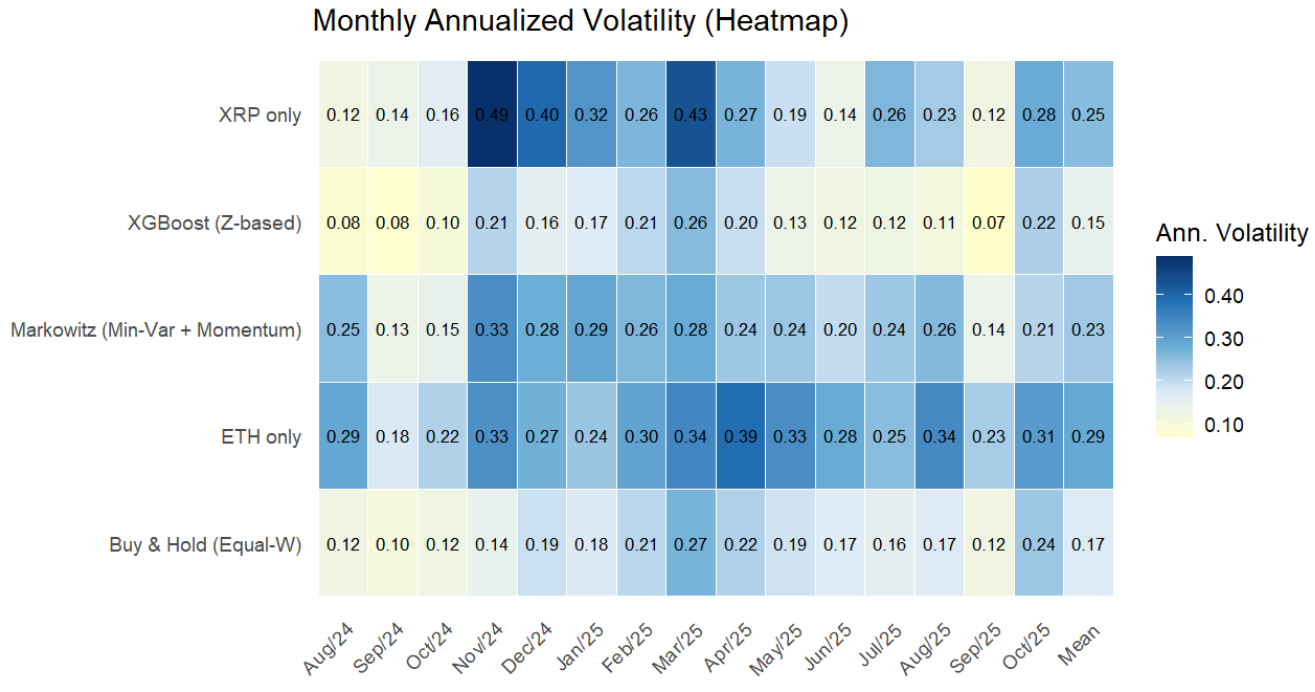

(b)

Figure 15. Heatmap of monthly compound returns and annualized volatility.

Figure 15a illustrates the monthly compounded returns in heatmap format for XGBoost, Markowitz, ETH/XRP-only allocations, and a buy-and-hold strategy, reporting mean values of –3.17%,

4.42%, –2.37%, –5.25%, and –7.52%. The XGBoost allocator exhibits frequent positive months with limited exposure to extreme negatives, while Markowitz and single-asset strategies combine occasional large gains with severe losses that erode geometric growth. Figure 15b reports monthly annualized volatility via heatmaps for XGBoost, Markowitz, ETH/XRP-only portfolios, and a buy-and-hold strategy, with observed mean values of 0.25, 0.15, 0.23, 0.29, and 0.17, respectively. The XGBoost allocator shows fewer high-volatility months than momentum and single-asset strategies, consistent with volatility scaling and portfolio-level risk budgeting that spreads risk rather than dollar notional values, improving the Sharpe and tail behavior. To advance portfolio design, tree-based learners and boosting algorithms (e.g., XGBoost) can be used to capture nonlinear dependencies among key drivers, including momentum, liquidity, and volatility. These interactions contribute to improved economic outcomes and higher risk-adjusted efficiency compared with traditional linear approaches [38]. Importantly, portfolio construction should maximize geometric welfare—i.e., long-run compounded growth—rather than optimize episodic arithmetic averages. Accordingly, a performance evaluation should emphasize the Sharpe ratio, CAGR (Compound Annual Growth Rate), and maximum drawdown, with drawdown control treated as a binding risk constraint; volatility scaling and crisis filters can be used to preserve compounding and attenuate tail risk [60]. To enhance cross-sectional selection, nonlinear tree-based learners such as XGBoost are well-suited to capturing higher-order interactions among momentum, liquidity, and volatility that are typically missed by linear specifications [38].

(4) Executive summary of findings

Across all reported metrics of Table 3, the XGBoost-based allocator using Z-scores is the only strategy that consistently converts signals into positive, risk-adjusted compounding. It achieves the highest terminal wealth (USD 17,812 from a USD 10,000 baseline; +78.1%), the best annualized Sharpe (2.08), the lowest maximum drawdown among peers (−20.9%), and a positive mean daily return (approximately 0.137%) with contained daily volatility (approximately 1.04%). In contrast, all comparators—rule-based momentum/Markowitz, equal-weight buy-and-hold, and single-asset ETH/XRP—exhibit negative risk- adjusted performance (Sharpe < 0), large drawdowns (−53% to −72%), and substantial capital erosion (−44% to −71%). The XGBoost-Z allocator outperforms the others by combining predictive cross-sectional learning with regime-aware risk safeguards, thereby maximizing risk-adjusted return and geometric compounding while bounding drawdowns—an actionable blueprint for portfolio engines in regime-shifting, high-volatility markets.

In addition to benchmarking traditional portfolio optimization, our findings highlight the risk management advantages of machine-intelligent approaches. The optimized portfolio exhibits a stable, mean reverting portfolio under daily minimum variance rebalancing and is idiosyncratically spiky but predominantly centered across constituents. Out-of-sample (13 Aug 2024–24 Oct 2025), the XGBoost model (Figure 16) achieves low standardized error (root mean square error (RMSE) ≈ 0.021, mean absolute error (MAE) ≈ 0.016) and high sign precision (79.27%), indicating that non-linear interactions among crypto provide actionable predictability for daily portfolio behaviour. SHAP-based diagnostics reveal that XRP and ETH consistently dominate global importance and drive local episodes in $f(x)$. These attributions provide audit-ready explanations that bridge statistical performance and economic interpretability, enabling more risk-aware portfolio allocation in modern crypto markets [49].

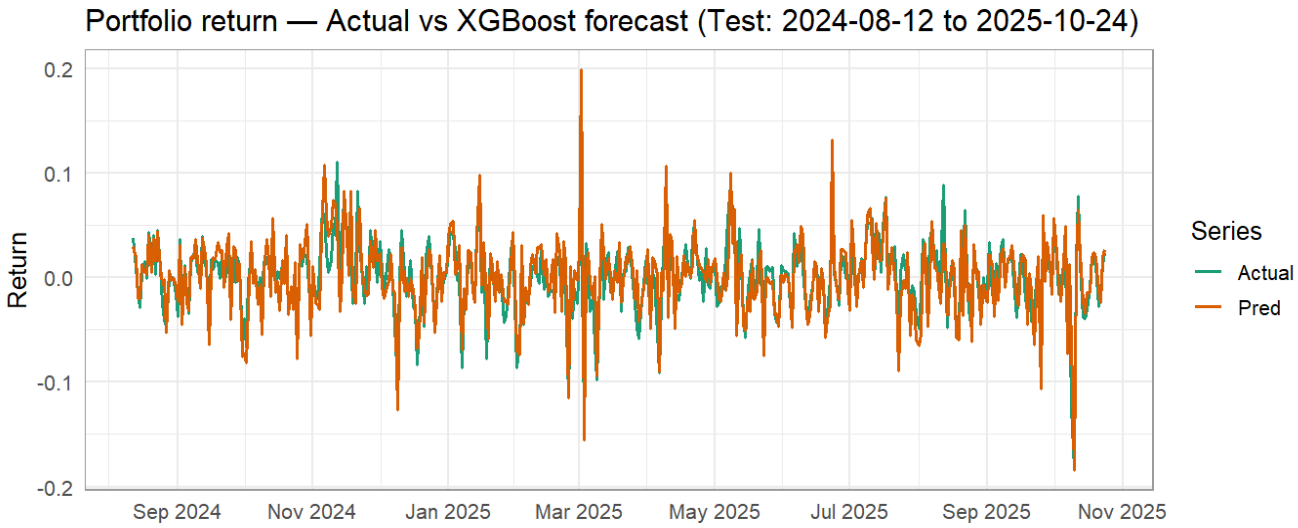

Figure 16. Portfolio return—Actual vs. XGBoost forecast (test: 2024-08-13 to 2025-10-24).

Baseline forecasts.

To contextualize the XGBoost results, we re-estimated three simple baselines on the same portfolio Z-score target and the same lagged asset Z-score features used in the main model and kept the study's train/test split. Based on the test set in Table 4, Figure 17a shows a random walk (level) forecast $\hat{Z}_{p,t}=Z_{p,t-1}$.

Table 3. Performance summary (backtest baseline P_0=\$10,000).

Metric	XGBoost (Z-based)	Markowitz (Min-Var + Momentum)	XRP only	ETH only	Buy & Hold (Equal weights)
Final value (USD)	**17,812**	5,574	4,886	4,129	2,868
Accumulated return (%)	**+78.1**	−44.3	−51.1	−58.7	−71.3
CAGR (%)	**61.8**	−38.6	−45.0	−52.2	−64.7
Sharpe (annualized)	**2.08**	−1.19	−1.26	−1.59	−3.79
MeanDaily (%)	**0.137**	−0.120	−0.147	−0.185	−0.277
SdDaily (%)	**1.04**	1.60	1.84	1.84	1.16
Max drawdown (%)	**−20.9**	−53.2	−62.5	−61.7	−72.3
Mean monthly ann. ret (%)	**2.29**	4.64	4.62	1.90	−0.278
Mean monthly ann. vol (%)	**14.9**	23.3	25.4	28.7	17.3

Table 3 reports the returns and volatilities in percentage (e.g., MeanDaily = 0.137%; SdDaily = 1.04%). Accumulated return is computed as (Final Value/ P_0−1) ×100%. Mean monthly ann. return is the arithmetic average of annualized monthly returns and is therefore not equivalent to the CAGR. Mean monthly ann. vol is the average of monthly volatility annualized from monthly observations.
The results achieve RMSE = 1.4402, MAE = 1.0857, and directional accuracy = 47.03%. An AR(1) specification $\hat{Z}_{p,t}=\alpha+\phi Z_{p,t-1}$ improves to RMSE = 0.9971, MAE = 0.7550, and directional accuracy = 51.03%. A linear model using the same 10 asset Z-scores as regressors delivers RMSE =

0.9951, MAE = 0.7582, and directional accuracy = 49.77%. As shown in Figure 17b, relative to the random walk, these linear/AR baselines reduce RMSE by ≈31% and MAE by ≈30%, with modest sign-accuracy increases of +4.0 percentage points (pp) (AR (1)) and +2.74 pp (linear).

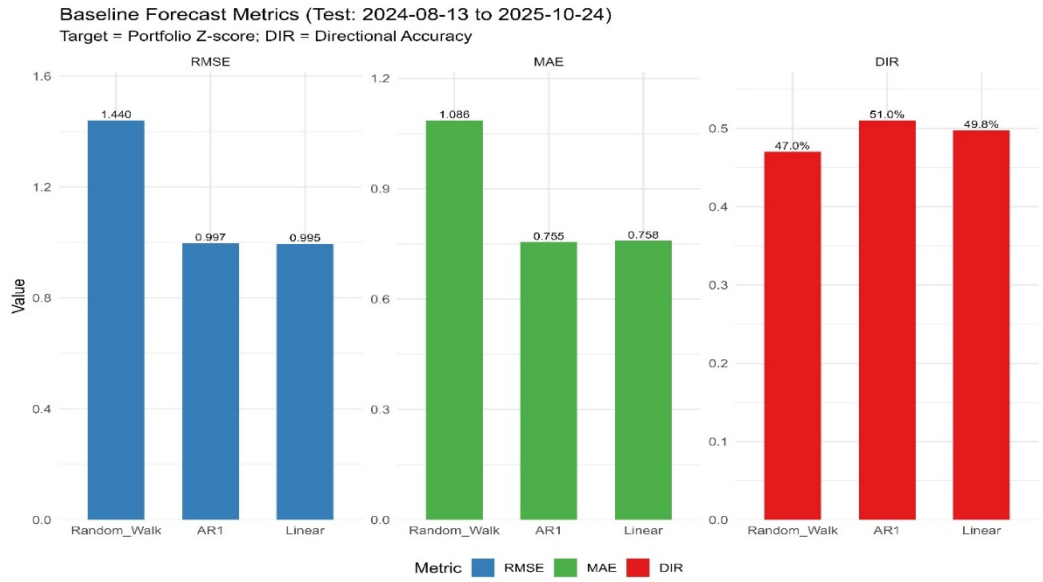

(a)

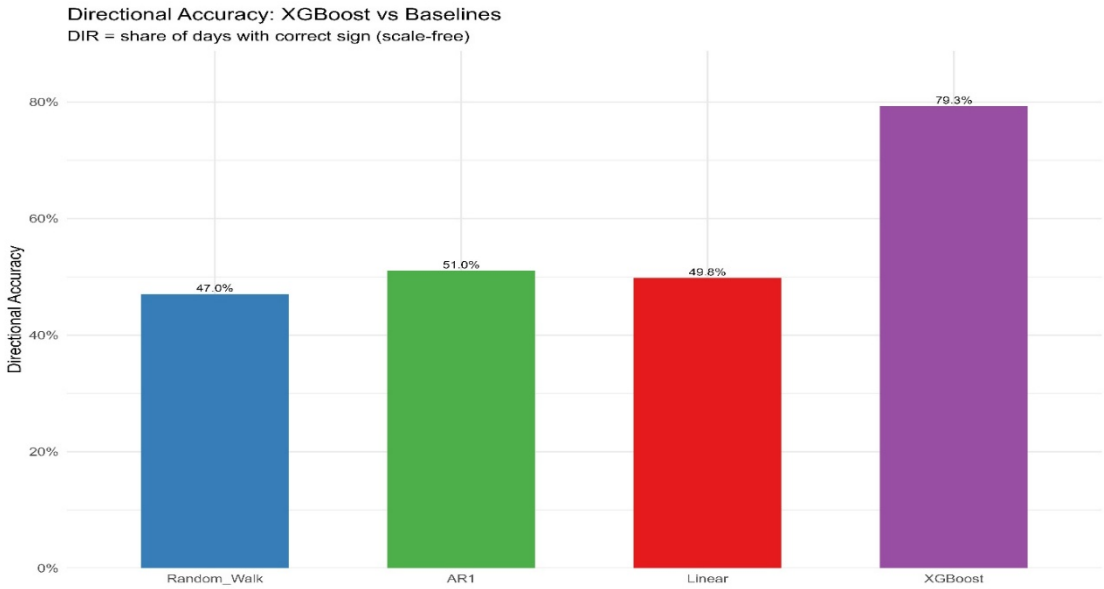

(b)

Figure 17. Test-sample DIR and uplift relative to RW.

Figure 17 reports out-of-sample directional accuracy (DIR) for the portfolio Z-score target and the uplift relative to the random walk benchmark. On the test set, random walk = 47.03%, linear = 49.77%, and AR (1) = 51.03%. The corresponding uplifts (in percentage points, pp) are computed as Uplift=DIR (model)−DIR(RW). Thus, linear: 49.77%−47.03%=+2.74 pp and AR (1): 51.03% − 47.03% = +4.00 pp.

Conditional performance (signal strength).

When the prior-day portfolio signal is stronger (at thresholds $|Z_{p,t-1}| \geq 0.5$ and $|Z_{p,t-1}| \geq 1.0$), errors rise for all methods (as expected), yet the AR (1) and linear models retain a clear edge over the random walk. For $|Z_{p,t-1}| \geq 0.5$, AR(1) results in RMSE = 1.0411, MAE = 0.7936, and directional accuracy (DIR) = 52.96%, versus the random walk's RMSE = 1.7072, MAE = 1.3332, DIR = 46.85%; for $|Z_{p,t-1}| \geq 1.0$, AR(1) delivers RMSE = 1.1365, MAE = 0.8839, and DIR = 58.77%, while the random walk records RMSE = 2.1743, MAE = 1.8240, DIR = 41.23%. The linear model is broadly similar to AR(1) in terms of the errors but slightly weaker on the signs in these bins. These conditional baselines address the reviewer's concern that sign accuracy can be inflated near zero: Its ability remains when $|Z|$ is large.

XGBoost vs. baselines.

Figure 16 reports XGBoost forecast performance on the test set (RMSE = 0.021068; MAE = 0.015602; directional accuracy = 79.27%).

Table 4. Baseline and conditional forecasting metrics (test sample).

Subsample	Threshold	Model	*n*	RMSE	MAE	DIR
Overall (test)	—	Random walk	—	1.4402	1.0857	0.4703
		AR(1)	—	0.9971	**0.7550**	**0.5103**
		Linear	—	**0.9951**	0.7582	0.4977
$\|Z_{p,t-1}\| \geq 0.5$	0.5	AR(1)	254	1.0411	**0.7936**	**0.5296**
		Linear	254	**1.0362**	0.7957	0.5000
		Random walk	254	1.7072	1.3332	0.4685
$\|Z_{p,t-1}\| \geq 1.0$	1.0	AR(1)	114	1.1365	**0.8839**	**0.5877**
		Linear	114	**1.1320**	0.8870	0.5175
		Random walk	114	2.1743	1.8240	0.4123

Table 4 reports RMSE, MAE, and DIR defined as the proportion of correct sign predictions). Here *n* denotes the number of observations in each subsample. Boldface indicates the best performance within each subsample (the lowest RMSE/MAE or highest DIR).

4.3. Robustness testing

On the same target and test window, our XGBoost model (Figure 15b) achieves DIR= 79.27%, a +28.24pp increase over the best simple baseline (51.03% for AR-(1)). This gap indicates a substantial incremental predictive content beyond mean-reversion and the linear structure, precisely when evaluated against appropriately strong baselines.

As a robustness check, we perform robustness tests using an alternative approach to measure spillover effects through correlation contagion testing and control the bivariate association with ETH vs. AI coins and the results are documented in Table 5. Interestingly, within the ETH vs. AI coins asset class pairs, the ETH-NEAR pair exhibits the strongest correlation, with non-crisis (x) and crisis (y) values of 0.6140 and 0.6057, respectively. We observe that among the ETH vs. AI coin pairs, the ETH-AKT pair shows the lowest correlation, with values of 0.3722 during non-crisis periods (x) and 0.4516 during crisis periods (y). Overall, for the ETH vs. AI coin asset class pairs, the p-values are less than the 1% significance level rejecting the null hypothesis of "no contagion from market i to market j". Accordingly, the findings in Table 5 suggest that we can confidently reject the null hypothesis of no contagion for all ETH vs. AI coin pairs in our sample, and ETH exhibits time-varying volatility spillovers to the five major AI coins. Overall, contagion denotes a regime shift in cross-market dependence (especially covolatility), after adjusting for crisis-time heteroskedasticity; it does not require the raw crisis correlation to exceed the non-crisis correlation.

Table 5. Correlation and contagion tests.

ETH (i) → AI Coin (j) → / Metric ↓	ETH (i)	NEAR(j)	FET(j)	RNDR(j)	INJ(j)	AKT(j)
Non-crisis (x) volatility (ETH)	2.87%					
Crisis (y) volatility (ETH)	5.06%					
Non-crisis (x) volatility (AI)		5.24%	6.49%	6.15%	5.87%	6.48%
Crisis (y)volatility (AI)		7.75%	7.77%	9.42%	7.76%	6.46%
Non-crisis(x) mean (ETH)	0.14%					
Crisis (y) mean (ETH)	0.13%					
Non-crisis (x) mean (AI)		0.20%	0.38%	0.42%	0.45%	0.45%
Crisis (y) mean (AI)		0.07%	0.06%	0.15%	0.03%	0.01%
Non-crisis (x) covolatility		-4.96	-4.32	-4.47	-4.50	-3.04
Crisis (y) covolatility		-2.88	-3.02	-2.31	-3.05	-2.40
Non-crisis (x) correlation		0.6140	0.5397	0.5573	0.5612	0.3722
Crisis (y) correlation		0.6057	0.6025	0.4347	0.5941	0.4516
Adjusted correlation		0.3961	0.3933	0.2638	0.3861	0.2757
Test statistic (χ^2)		164.59^{***}	72.01^{***}	209.15^{***}	87.13^{***}	23.84^{***}
p-value		0.000	0.000	0.000	0.000	0.000
Contagion detected		Yes	Yes	Yes	Yes	Yes

Table 5 reports sample sizes of 590 non-crisis observations (x) and 798 crisis observations (y), making the regime split explicit. In the baseline specification, crisis days are identified deterministically using pre-specified external event windows: All dates within the COVID-19 window (October 25, 2020–December 31, 2022) are coded as crisis, with all remaining dates coded as non-crisis. The χ^2 statistic corresponds to the Fry-McKibbin and Hsiao [51] contagion test (see

Eq. 3.35). It tests whether linkages differ materially between regimes. *** denotes significance at the 1% level.

5. Conclusions and policy implications

The results illustrated in Figures 3 and 4 have significant implications for key crypto-holders regarding connectedness. For market participants, it is essential to understand the significant spillovers within the AI coins and green cryptocurrency markets. Identifying green cryptocurrencies as primary transmitters of return shocks and recognizing the AI coin markets' receptiveness aids in developing robust investment strategies. Portfolio managers need to remain alert due to the intense factors currently driving return transmission. Risk management strategies should be flexible and account for the interconnectedness between AI coin and green cryptocurrency markets. Moreover, regulators should prioritize transparency and effective information sharing to enable cryptocurrency investors to make informed decisions amidst the interconnected dynamics highlighted by our static connectedness findings. Empirically, in the preceding result, ETH's role as a net transmitter of volatility to both green and AI-crypto segments amplifies its cross-asset impact, while XRP's deep liquidity, high turnover, and recurrent momentum volatility cycles make its contributions both large in magnitude and consistently active under daily rebalancing. In addition, through the dynamic network connectedness analysis, the study suggests that ETH acted as a volatility transmitter to most of the other green cryptocurrencies and AI coins with a positive contribution. Complementary SHAP waterfall analysis further identifies ETH as the dominant contributor within the optimized cryptocurrency portfolio, with a Shapley value of 0.4873.

5.1. Policy implications

The study confirms that spillovers from green cryptocurrency to AI tokens are consistent with financing or shared investor base narratives, but our evidence is reduced form and does not identify a policy mechanism. Motivated by the recent surge of net-zero carbon emission activism, we analyze volatility transmission between five green cryptocurrencies and five AI tokens. To this end, we use a TVP-VAR connectedness framework to capture the time-varying pattern of spillovers. We then combine this framework with machine-intelligent portfolio optimization to evaluate risk-adjusted allocation outcomes across green and AI cryptocurrency assets. The results reveal substantial interconnectedness between the two market segments, with green cryptocurrencies emerging, on balance, as net transmitters of volatility spillovers to AI tokens. Our findings carry practical and policy relevance. However, these implications should be interpreted as being in reduced form rather than causal. For investors and risk managers, the documented time variation in connectedness suggests that short-horizon spillovers may erode diversification benefits during episodes of elevated market volatility. This pattern underscores the value of flexible hedging strategies and horizon-sensitive portfolio rebalancing. For market surveillance, episodic cross-segment dependence underscores the value of connectedness and tail-risk monitoring. Methodologically, the machine-learning framework, complemented by SHAP-style diagnostics, provides an auditable approach to real-time risk-signal attribution.

5.2. Key takeaways and implications for portfolio design

SHAP's guarantees—local accuracy, consistency, and missingness—and efficient TreeSHAP implementations make it a gold standard for explaining gradient-boosted trees [50]. Practically,

diagnostics support evidence-based asset selection and risk budgeting, regime-aware Markowitz diversification complemented by SHAP heatmaps, and tail governance via drawdown caps, stop-losses, and shock scenarios [58, 59]. Empirically, naïve diversification is insufficient: equal-weight portfolios are drift-exposed (Sharpe = −3.79; maximum drawdown (MDD) = −72.3%). By contrast, the XGBoost Z-score allocator jointly controls drift, variance, and drawdown, achieving Sharpe = 2.08, terminal value = \$17,812 (+78.1%), and the MDD = −20.9%. Nonlinear selectivity curbs momentum crashes and idiosyncratic concentration, and evaluation must remain coherent across Sharpe, terminal wealth, and drawdown metrics.

For completeness, we note at the outset that our connectedness and machine-learning analyses are based on token return dynamics and model-implied dependence. Policy variables are neither directly observed nor instrumented in the current design. Any references to financing, regulatory narratives, or information frictions are therefore explicitly framed as hypotheses or interpretive commentary, rather than as causal inferences.

5.3. The limited and future directions for sustainability/AI cryptocurrencies

This paper may help inform future research on sustainability and AI cryptocurrencies, particularly as AI technologies continue to reshape a wide range of industries. These developments are likely to encourage firms and policymakers to adopt new training strategies in response to the evolving skill demands of a sustainability economy. Notwithstanding these contributions, several limitations remain and point to important directions for future research, as discussed below.

First, establishing policy transmission requires exogenous policy shocks or observable policy proxies (e.g., carbon prices, ESG indices, timestamped regulatory announcements), event-study windows, or structural identification (e.g., instruments, narrative-shock designs).

Second, our connectedness measures and XGBoost attributions (e.g., SHAP) are associational rather than causal; embedding causal identification within these frameworks is an important direction for subsequent work.

Use of AI tools declaration

The authors declare they have not used AI tools in the creation of this article.

Acknowledgments

The authors thank the two anonymous reviewers for their constructive comments and suggestions, which substantially improved the quality and clarity of the manuscript.

Conflict of interest

The authors declare no competing interests.

Author contributions

All authors contributed equally to the study conception, and manuscript drafting, revision, and final approval collectively herein.

References

1. D. B. Olawade, O. Z. Wada, A. C. David-Olawade, O. Fapohunda, A. O. Ige, J. Ling, Artificial intelligence potential for net zero sustainability: Current evidence and prospects, *Next Sustainability*, **4** (2024), 100041. https://doi.org/10.1016/j.nxsust.2024.100041
2. T. Lim, Environmental, social, and governance (ESG) and artificial intelligence in finance: State-of-the-art and research takeaways, *Artif. Intell. Rev.*, **57** (2024), 76. https://doi.org/10.1007/s10462-024-10708-3
3. R. Patel, S. Kumar, E. Bouri, N. Iqbal, Spillovers between green and dirty cryptocurrencies and socially responsible investments around the war in Ukraine, *Int. Rev. Econ. Finance*, **87** (2023), 143–162. https://doi.org/10.1016/j.iref.2023.04.013
4. M. Zeng, W. Zhang, Green finance: The catalyst for artificial intelligence and energy efficiency in Chinese urban sustainable development, *Energy Econ.*, **139** (2024), 107883. https://doi.org/10.1016/j.eneco.2024.107883
5. L. Pham, T. L. D. Huynh, W. Hanif, Time-varying asymmetric spillovers among cryptocurrency, green and fossil-fuel investments, *Glob. Finance J.*, **58** (2023), 100891. https://doi.org/10.1016/j.gfj.2023.100891
6. B. Bedowska-Sojka, A. Kliber, Do investors in dirty and clean cryptocurrencies care about energy efficiency in the same way? *Finance Res. Lett.*, **67** (2024), 105852. https://doi.org/10.1016/j.frl.2024.105852
7. A. Kliber, B. Bedowska-Sojka, Proof-of-work versus proof-of-stake coins as possible hedges against green and dirty energy, *Energy Econ*., **138** (2024), 107820. https://doi.org/10.1016/j.eneco.2023.107820
8. A. Yakovenko, Solana: A new architecture for a high performance blockchain v0.8.13, White paper, (2018). Available from: http://tinyurl.com/hmks9mx7.
9. S. Alizadeh, M. Khabbazian, Solana's transaction network: Analysis, insights, and comparison, *EPJ Data Sci.*, **14** (2025), 1–16.
10. T. L. D. Huynh, E. Hille, M. A. Nasir, Diversification in the age of the 4th industrial revolution: The role of artificial intelligence, green bonds and cryptocurrencies, *Technol. Forecast. Soc. Change*, **159** (2020), 120188. https://doi.org/10.1016/j.techfore.2020.120188
11. S. Demiralay, H. G. Gencer, S. Bayraci, How do artificial intelligence and robotics stocks co-move with traditional and alternative assets in the age of the 4th industrial revolution? Implications and insights for the COVID-19 period, *Technol. Forecast. Soc. Change*, **171** (2021), 120989. https://doi.org/10.1016/j.techfore.2021.120989
12. F. Jareno, I. Yousaf, Artificial intelligence-based tokens: Fresh evidence of connectedness with artificial intelligence-based equities, *Int. Rev. Financ. Anal.,* **89** (2023), 102826. https://doi.org/10.1016/j.irfa.2023.102826
13. M. Abdullah, P. K. Sarker, E. J. A. Abakah, A. K. Tiwari, M. Z. Rehman, Tail risk intersection between tech-tokens and tech-stocks, *Glob. Financ. J.*, **61** (2024), 100989. https://doi.org/10.1016/j.gfj.2023.100989
14. A. Husain, K. J. Yii, C. C. Lee, Are green cryptocurrencies really green? New evidence from wavelet analysis, *J. Clean. Prod*., **417** (2023), 137985. https://doi.org/10.1016/j.jclepro.2023.137985

15. K. Duan, Y. Zhao, A. Urquhart, Y. Huang, Do clean and dirty cryptocurrencies connect with financial assets differently? The role of economic policy uncertainty, *Energy Econ*., **127** (2023), 107079. https://doi.org/10.1016/j.eneco.2023.107079
16. M. A. Naeem, T. T. H. Nguyen, S. Karim, B. M. Lucey, Extreme downside risk transmission between green cryptocurrencies and energy markets: The diversification benefits, *Finance Res. Lett*., **58** (2023), 104263. https://doi.org/10.1016/j.frl.2022.104263
17. F. Ali, M. U. Khurram, A. Sensoy, X. V. Vo, Green cryptocurrencies and portfolio diversification in the era of greener paths, *Renewable Sustainable Energy Rev.*, **191** (2024), 114137. https://doi.org/10.1016/j.rser.2023.114137
18. J. Almeida, T. C. Gonçalves, The AI revolution: Are crypto markets more efficient after ChatGPT 3? *Finance Res. Lett*., **66** (2024), 105608. https://doi.org/10.1016/j.frl.2024.105608
19. A. Saggu, L. Ante, The influence of ChatGPT on artificial intelligence related crypto assets: Evidence from a synthetic control analysis, *Finance Res. Lett*., **55** (2023), 103993. https://doi.org/10.1016/j.frl.2023.103993
20. S. Chipolina, Bitcoin leaves the rest of the crypto market behind, FT Cryptofinance Newsletter, (2023). Available from: https://www.ft.com/content/5160b007-5e68-423d-8a6c-a0fdef6199f4?syn-25a6b1a6=1.
21. L. Ante, E. Demir, The ChatGPT effect on AI-themed cryptocurrencies, *Econ. Bus. Lett*., **13** (2024), 29–38. https://doi.org/10.17811/ebl.14.1.2024.29-38
22. C. Stoll, L. Klaassen, U. Gallersdorfer, The carbon footprint of Bitcoin, *Joule*, **3** (2019), 1647–1661. https://doi.org/10.1016/j.joule.2019.05.012
23. B. Ren, B. Lucey, A clean, green haven?—Examining the relationship between clean energy, clean and dirty cryptocurrencies, *Energy Econ*., **109** (2022), 105951. https://doi.org/10.1016/j.eneco.2022.105951
24. L. Pham, S. Karim, M. A. Naeem, C. Long, A tale of two tails among carbon prices, green and non-green cryptocurrencies, *Int. Rev. Financ. Anal*., **82** (2022), 102139. https://doi.org/10.1016/j.irfa.2022.102139
25. K. S. Chen, W. C. Ong, Dynamic correlations between Bitcoin, carbon emission, oil and gold markets: New implications for portfolio management, *AIMS Math*., **9** (2024), 1403–1433. https://doi.org/10.3934/math.2024069
26. S. Long, H. Tian, Z. Li, Dynamic spillovers between uncertainties and green bond markets in the US, Europe, and China: Evidence from the quantile VAR framework, *Int. Rev. Financ. Anal*., **84** (2022), 102416. https://doi.org/10.1016/j.irfa.2022.102416
27. K.C. Lu, K.S. Chen, Uncovering information linkages between Bitcoin, sustainable finance and the impact of COVID-19: Fractal and entropy analysis, *Fractal Fract*., **7** (2023), 424. https://doi.org/10.3390/fractalfract7060424
28. J. Wu, J. P. Li, C. W. Su, Can green bond hedges climate policy uncertainty in the United States? *Econ. Anal. Policy*, **82** (2024), 1158–1176. https://doi.org/10.1016/j.eap.2023.08.015
29. I. Yousaf, O. M. Ohikhuare, Y. Li, Y. Li, Interconnectedness between electricity and artificial intelligence-based markets during the crisis periods: Evidence from the TVP-VAR approach, *Energy Econ*., **139** (2024), 107885. https://doi.org/10.1016/j.eneco.2024.107885
30. S. B. Jabeur, G. Gozgor, H. Rezgui, K. S. Mohammed, Dynamic dependence between quantum computing stocks and Bitcoin: Portfolio strategies for a new era of asset classes, *Int. Rev*. *Financ. Anal.*, **95** (2024), 103478. https://doi.org/10.1016/j.irfa.2023.103478

31. C. C. Wu, W. P. Chen, What's an AI name worth? The impact of AI ETFs on their underlying stocks, *Finance Res. Lett*., **46** (2022), 102474. https://doi.org/10.1016/j.frl.2021.102474
32. A. K. Tiwari, E. J. A. Abakah, T. L. Le, D. I. Leyva-de la Hiz, Markov-switching dependence between artificial intelligence and carbon price: The role of policy uncertainty in the era of the 4th industrial revolution and the effect of COVID-19 pandemic, *Technol. Forecast. Soc. Change*, **163** (2021), 120434. https://doi.org/10.1016/j.techfore.2020.120434
33. S. Sharma, A. K. Tiwari, S. Nasreen, Are FinTech, robotics, and blockchain index funds providing diversification opportunities with emerging markets? Lessons from pre and post outbreak of COVID-19, *Electron. Commer. Res*., **24** (2024), 341–370. https://doi.org/10.1007/s10660-022-09611-2
34. E. Jacquier, A. Kane, A. J. Marcus, Geometric or Arithmetic Mean: A Reconsideration, *Financ. Anal. J*., **59** (2003), 46–53. https://doi.org/10.2469/faj.v59.n6.2574
35. A. Moreira, T. Muir, Volatility-managed portfolios, *J. Finance*, **72** (2017), 1611–1644. https://doi.org/10.1111/jofi.12513
36. C. R. Harvey, E. Hoyle, R. Korgaonkar, S. Rattray, M. Sargaison, O. Van Hemert, The impact of volatility targeting, *SSRN Electron. J*., (2018), 3175538.
37. K. Daniel, T. J. Moskowitz, Momentum crashes, *J. Financ. Econ*., **122** (2016), 221–247. https://doi.org/10.1016/j.jfineco.2015.12.002
38. S. Gu, B. Kelly, D. Xiu, Empirical asset pricing via machine learning, *Rev. Financ. Stud*., **33** (2020), 2223–2273.https://doi.org/10.1093/rfs/hhaa009
39. L. Chen, M. Pelger, J. Zhu, Deep learning in asset pricing, *Manage. Sci*., **70** (2024), 714–750. https://doi.org/10.1287/mnsc.2023.4695
40. J. Jang, N. Seong, Deep reinforcement learning for stock portfolio optimization by connecting with modern portfolio theory, *Expert Syst. Appl*., **218** (2023), 119556. https://doi.org/10.1016/j.eswa.2023.119556
41. F. X. Diebold, K. Yilmaz, Better to give than to receive: Predictive directional measurement of volatility spillovers, *Int. J. Forecast*., **28** (2012), 57–66. https://doi.org/10.1016/j.ijforecast.2011.02.006
42. H. H. Pesaran, Y. Shin, Generalized impulse response analysis in linear multivariate models, *Econ. Lett*., **58** (1998), 17–29. https://doi.org/10.1016/S0165-1765(97)00214-0
43. N. Antonakakis, I. Chatziantoniou, D. Gabauer, Refined measures of dynamic connectedness based on time-varying parameter vector autoregressions, *J. Risk Financ. Manage*., **13** (2020), 84. https://doi.org/10.3390/jrfm13040084
44. Q. Ji, E. Bouri, C. K. M. Lau, D. Roubaud, Dynamic connectedness and integration in cryptocurrency markets, *Int. Rev. Financ. Anal.*, **63** (2019), 257–272. https://doi.org/10.1016/j.irfa.2018.12.002
45. I. O. Fasanya, O. Oyewole, T. Odudu, Returns and volatility spillovers among cryptocurrency portfolios, *Int. J. Manag. Financ*., **17** (2021), 327–341. https://doi.org/10.1108/IJMF-02-2019-0074
46. G. Koop, M. H. Pesaran, S. M. Potter, Impulse response analysis in nonlinear multivariate models, *J. Econom*., **74** (1996), 119–147. https://doi.org/10.1016/0304-4076(95)01753-4
47. K. Phoon, F. Koh, Robo-Advisors and wealth management, *J. Altern. Invest*., **20** (2017), 79–94. https://doi.org/10.3905/jai.2018.20.3.079

48. T. Chen, C. Guestrin, XGBoost: A scalable tree boosting system, in *Proceedings of the 22nd ACM SIGKDD International Conference on Knowledge Discovery and Data Mining*, (2016), 785–794. https://doi.org/10.1145/2939672.2939785
49. S. M. Lundberg, S. Lee, A unified approach to interpreting model predictions, in *Advances in Neural Information Processing Systems*, **30** (2017), 4765–4774.
50. S. M. Lundberg, G. Erion, H. Chen, A. DeGrave, J. M. Prutkin, B. Nair, et al., From local explanations to global understanding with explainable AI for trees, *Nat. Mach. Intell.*, **2** (2020), 56–67. https://doi.org/10.1038/s42256-019-0138-9
51. R. Fry-McKibbin, C. Y. L. Hsiao, Extremal dependence tests for contagion, *Econ. Rev.*, **37** (2018), 626–649. https://doi.org/10.1080/07474938.2018.1452356
52. K. J. Forbes, R. Rigobon, No contagion, only interdependence: Measuring stock market co-movements, *J. Finance*, **57** (2002), 2223–2261. https://doi.org/10.1111/0022-1082.00494
53. R. Fry, V. L. Martin, C. Tang, A new class of tests of contagion with applications, *J. Bus. Econ. Stat.*, **28** (2010), 423–437. https://doi.org/10.1198/jbes.2009.08098
54. P. K. Narayan, Understanding exchange rate shocks during COVID-19, *Finance Res. Lett.*, **45** (2022), 102181.https://doi.org/10.1016/j.frl.2021.102181
55. S. Khademalomoom, P. K. Narayan, Intraday effects of the currency market, *J. Int. Financ. Mark. Inst. Money*, **58** (2019), 65–77. https://doi.org/10.1016/j.intfin.2018.09.008
56. J. Barunik, T. Krehlik, Measuring the frequency dynamics of financial connectedness and systemic risk, *J. Financ. Econom.*, **16** (2018), 271–296. https://doi.org/10.1093/jjfinec/nby001
57. H. Markowitz, Portfolio selection, *J. Finance*, **7** (1952), 77–91. https://doi.org/10.2307/2975974
58. H. T. Wu, M. L. Yueh, Cryptocurrency risk management using Levy processes and time-varying volatility, *Rev. Quant. Financ. Account.*, **66** (2026), 33–61. https://doi.org/10.1007/s11156-025-01393-6
59. A. Phiri, I. Anyikwa, A multiscale analysis of returns and volatility spillovers in cryptocurrency markets: A post-COVID perspective, *Invest. Anal. J.*, **54** (2025), 21–41. https://hdl.handle.net/10520/ejc-invest_v54_n1_a21
60. T. J. Moskowitz, Y. H. Ooi, L. H. Pedersen, Time series momentum, *J. Financ. Econ.*, **104** (2012), 228–250. https://doi.org/10.1016/j.jfineco.2011.11.003

AIMS Press